Technical Abstract

Driven monopiles are often the preferred foundation type for offshore wind turbines in shallow water applications. The designer must limit the accumulated rotation of the structure within its lifetime, which occurs due to one-way cyclic loading acting on the tower. To limit the rotation and optimise the foundation design, the natural frequency of the structure should be designed to be outside of the range of forcing frequencies related to wave, wind, and rotor passing effects, however the non-linear nature of the soil makes prediction of the natural frequency difficult. There remains no validated method for the design of offshore rigid monopiles, and design codes for lateral stiffness developed by the oil industry for slender piles are often adopted, despite being used outside of their verified range. Caution is therefore advised when predicting the response at small lateral displacements, as with natural frequency calculations.

This report investigates and evaluates different methods for finding the natural frequency of model monopiles in 1-g testing, predominantly in dry sand. A simple model for predicting the natural frequency is developed using existing design codes, and its limitations are discussed and its results compared with measured natural frequencies.

Impulse tests were found to require isolation of the ‘correct’ natural frequency, this was achieved by comparison with reference tests on the pile, and noting the effect of additional mass and modification of the impulse application point. Careful study using Fourier analysis was then required. Impulse tests were found to give near to an upper bound on the natural frequency, as the soil stiffness increases as the response dies down. Low force amplitude harmonic tests of two-way cyclic loading agreed well with the results of impulse tests. As the force amplitude was increased, the natural frequency dropped, suggesting the soil stiffness is non-linear even at low strain levels. The natural frequency of the pile-soil system was found to change with variations in the soil density and pile embedment. An initial gain of around 10% in stiffness was found with cyclic loading, but the load level was insufficient to find a long-term degradation or enhancement of the stiffness. Comparisons between tests in sand and clay were found to be difficult to make due to differences in their expected lateral stiffness profile with depth.

The model developed provides expressions for calculating the natural frequency of the rotational and horizontal rigid body modes of the embedded monopile. This underestimated the natural frequency for tests in both loose and dense sand by up to 30%. For piles with a lower embedment and therefore a higher eccentricity of loading, a coupling between the two rigid body modes was predicted, with experimental data appearing to confirm this. The main limitations of the model are that it ignores shear at the base of the pile and its reliance on a constant initial stiffness of the soil, assumed to be independent of diameter, and shown by tests to vary even at low displacements.

Further investigation is required into the effect of pile diameter on the natural frequency, and centrifuge tests should be carried out for comparison with field data and results from finite element analysis.

Contents

Technical Abstract ..... **i**

Contents ..... **iii**

Nomenclature ..... **iv**

1 **Introduction** **1**
- **1.1 Background to Offshore Wind Turbines** **1**
- **1.2 Problem Definition** **3**
- **1.3 Project Objectives** **5**

2 Literature Review **6**
- **2.1 Lateral Loading of Piles** **6**
- **2.2 Monopile Foundations** **9**
- **2.3 Predicting the Natural Frequency of Flexible and Rigid Piles** **12**
- **2.4 Experimental Modelling and Dimensional Analysis** **14**
- **2.5 Conclusions** **14**

3 Experimental Methods **15**
- **3.1 Experimental Setup** **15**
- **3.2 Soil** **16**
- **3.3 Impulse Response** **17**
- **3.4 Harmonic Response** **18**
  - 3.4.1 Eccentric Mass Vibrator 18
  - 3.4.2 Piezo-electric Actuator 19
- **3.5 Instrumentation, Measurement and Analysis** **21**
- **3.6 Experimental Setup** **21**

4 Model for Predicting the Natural Frequency **23**

5 Impulse Response **26**
- **5.1 Cantilever Tests** **26**
- **5.2 Loose Sand** **28**
- **5.3 Dense Sand** **33**
- **5.4 Reduced Embedment** **35**
- **5.5 Comparison with Model** **35**
- **5.6 Evaluation of Impulse Tests** **35**

6 Harmonic Tests **36**
- **6.1 Eccentric Mass Vibrator** **36**
- **6.2 Piezo-electric Actuator** **37**
  - 6.2.1 Cantilever Tests 37
  - 6.2.2 Loose Sand Tests 39
  - 6.2.3 Clay Tests 42

7 Limitations of Small-Scale Models **44**

8 Conclusions **45**
- **8.1 Impulse Tests** **45**
- **8.2 Harmonic Tests** **46**
- **8.3 Suggestions for Further Work** **46**

9 References **47**

A Risk Assessment Retrospective **48**

Nomenclature

D	Pile diameter	[m]
E_s	Stiffness of soil	[Nm^{-2}]
E_P	Young's modulus of pile	[Nm^{-2}]
G	Shear modulus of soil	[Nm^{-2}]
H	Applied horizontal load	[N]
I_P	Pile second moment area about its diameter	[m^4]
K_{soil}	Equivalent stiffness of soil	[Nm^{-1}]
L	Embedded length of pile	[m]
M	Moment applied at pile head	[Nm]
M_{eq}	Equivalent mass of pile	[kg]
V	Applied vertical load	[N]
e	Load eccentricity	[m]
f_n	Fundamental natural frequency	[Hz]
$f_{sampling}$	Sampling frequency of data logger	[Hz]
k	Initial modulus of subgrade reaction	[Nm^{-3}]
m	Mass of pile	[kg]
m_{top}	Added mass at top of pile	[kg]
m_{total}	Total mass of pile system and soil plug	[kg]
p	Lateral resistance/unit length	[Nm^{-1}]
t	Pile wall thickness	[m]
y	Lateral displacement	[m]
y_{top}	Pile head lateral displacement	[m]
z	Depth below soil surface	[m]
z_{crit}	Depth of rotation point	[m]
ζ	Damping ratio	[/]

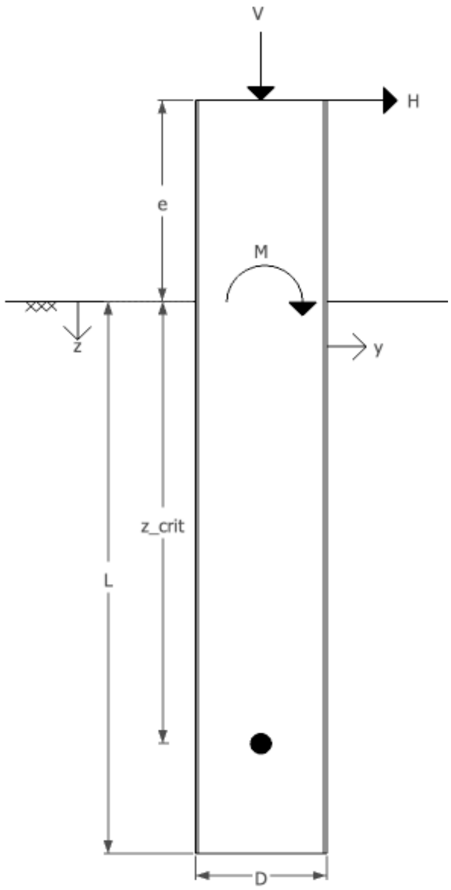

1 Introduction

1.1 Background to Offshore Wind Turbines

With the depletion of natural resources traditionally used for power generation such as oil and natural gas, as well as the increasing costs of extracting them, sources of renewable energy are becoming an increasingly attractive proposition. Renewable energy has the advantage of reduced CO_2 emissions relative to fossil fuels, and rising levels of CO_2 in the atmosphere have contributed towards climate change and global warming. The National Grid seven-year statement issued in 2010 predicted a peak demand in UK power of 58 GW in 2012, with an anticipated total power generating capacity of 89 GW. The government has set a target of 20% of the UK's energy demands being supplied by renewable energy by 2020, in order to meet EU directives on renewables. Further to this, the UK is targeting a reduction in CO_2 emissions of 60% by 2050 (Byrne & Houlsby, 2003).

Wind turbines are seen as an economical and reliable source of energy, and a large number of potential sites are available in the UK for wind farms. Data from the British Wind Energy Association (BWEA) in Table 1.1 shows that the current capacity in the UK from wind turbines is 6.61 GW, with another 3.80 GW under construction. Onshore developments are often met by opposition from local residents on aesthetic grounds, and further advantages of offshore wind turbines are that larger structures with a higher generation capacity are possible, and that the wind is more consistent (Byrne & Houlsby, 2003). As a result, most planned developments are offshore, an example being Gunfleet Sands, shown in Figure 1.1. With each individual turbine producing up to 5 MW of power, it is clear that a large number will be required to meet the government targets.

Table 1.1. Capacity of Wind Turbines in the UK (BWEA)

	Offshore Capacity	Onshore Capacity	Total Capacity
Current (GW)	1.86	4.76	6.61
Under Construction (GW)	2.36	1.44	3.80

Byrne & Houlsby (2003) estimate that the foundations for offshore wind turbines account for around 35% of the total cost. It is therefore very important to optimise the foundation design, and where possible reduce the quantity of materials used and the time taken for installation. The range of soil types around the UK coastline means that the same foundation is unlikely to be appropriate everywhere.

Figure 1.1. Gunfleet Sands Wind Farm (Dong Energy)

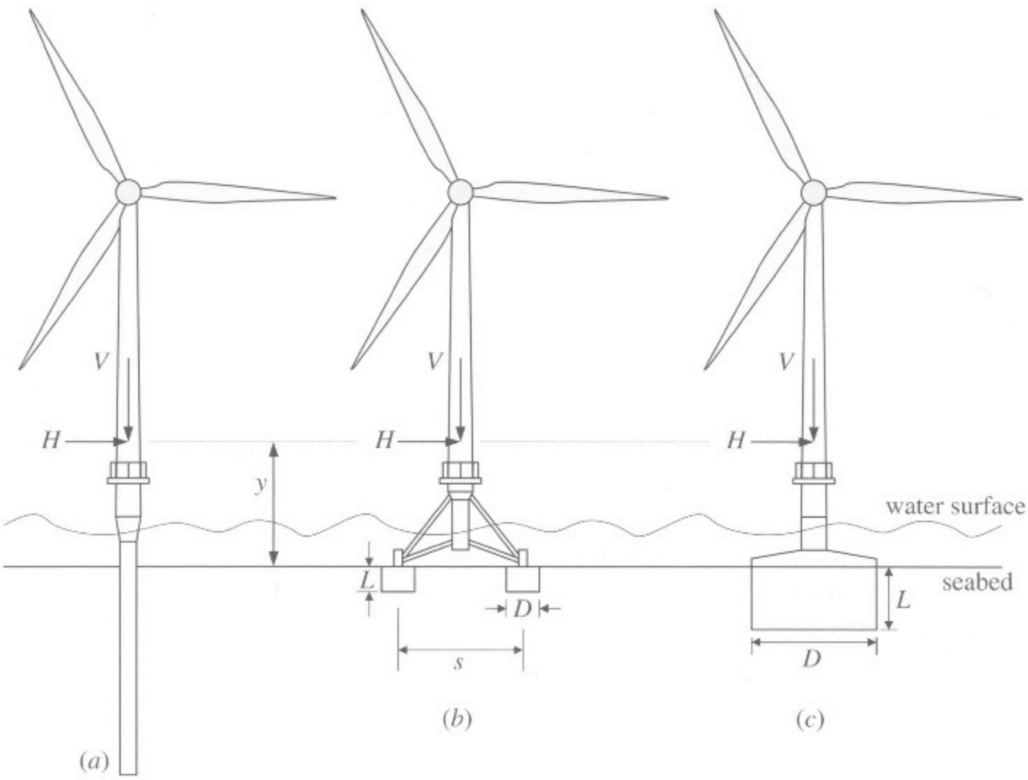

Figure 1.2. Foundation design options: (a) Monopile (b) Suction caisson multipod (c) Suction caisson monopod. (Byrne & Houlsby, 2003)

Figure 1.2 shows three typical foundation designs considered for wind turbine foundations in shallow water of around 20 m depth. Options (b) and (c) are both caisson foundations which use a pressure differential during installation. Material and installation costs are low, but they do not make use of stronger soil available deeper below the seabed, and the surface is susceptible to scour and erosion. For option (b) the vertical capacity of each 'pod' tends to be critical, whereas for option (c) the overturning capacity is critical. The monopile has been the favoured design for shallow water by the industry due to the existence of well-established procedures for installation and the availability of jack-up rigs used for installation from the oil industry. A monopile, shown in Figure 1.3, consists of a hollow steel tube of 4 to 6 m diameter, which is driven 20 to 30 m into the ground (LeBlanc, 2004). Although material and installation costs are high, especially if preliminary drilling is required, they remain economical for shallow water. For larger wind turbines in relatively deeper water, it is thought monopiles of up to 7.5 m diameter are possible (Achmus *et al.*, 2009). As will be shown in the next section, their design is governed by the horizontal capacity, serviceability and fatigue limit states.

Figure 1.3. Monopile foundation pre-installation (Dong Energy)

1.2 Problem Definition

Byrne & Houlsby (2003) observe that for most offshore sites around the UK, the surface soil consists of sandy deposits, in some areas underlain by clay. This is the case for a 3 MW Vestas turbine at Kentish Flat investigated by Bhattacharya *et al*. (2010), which was found to have an average soil shear modulus of 80 MPa.

Offshore sites tend to be susceptible to more extreme environmental conditions than onshore, and due to their length and slenderness wind turbines tend to be dynamically sensitive structures. Byrne & Houlsby (2003) found that the typical maximum vertical load applied to a wind turbine foundation for a 3.5 MW turbine is 6 MN, as well as a horizontal load of 4 MN at 30 m eccentricity, as shown in Figure 1.4. In the serviceability state, wind loading of 1 MN is applied at the hub (90 m above the seabed) and wave loading of 1±2 MN is applied at around 10 m above the seabed. Assuming the wind and wave loads are in the same direction, this leads to a design horizontal load of 2±2 MN, and a design moment of 100±20 MN. Horizontal and moment loading are therefore more critical than vertical loading.

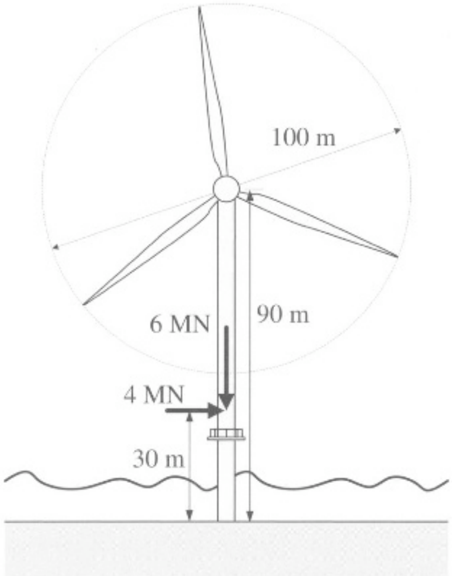

Figure 1.4. Typical design loads on an offshore wind turbine (Byrne & Houlsby, 2003)

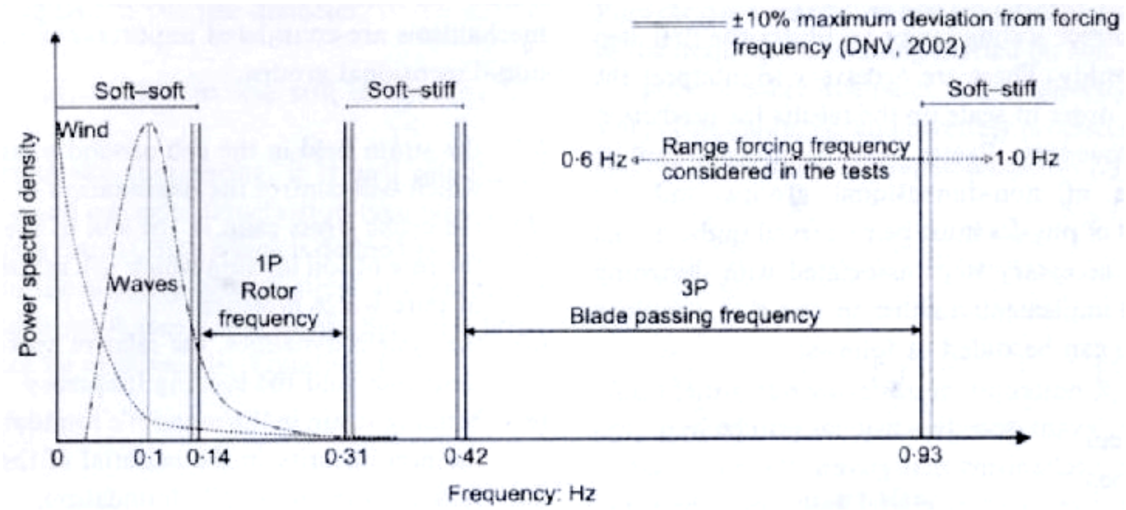

Figure 1.5. Forcing frequencies acting on a wind turbine (Bhattacharya *et al.*, 2010)

The cyclic loads applied set up a range of driving frequencies shown in Figure 1.5. Short duration wind loading consists of a mean speed with a fluctuating gust component of frequency 0.02 Hz (Adhikari & Bhattacharya, 2012). Wave loading is in the range of 0.04 to 0.1 Hz, and a '1P' rotor frequency is set up by the rotating blades. For a three-bladed structure a '3P' passing frequency is set up in the upper part of the tower, as each blade shadows it from the wind when it passes by. Det Norske Veritas (DNV) guidelines suggest a ±10% deviation from these forcing frequencies for design.

The natural frequency of the system should be designed to be outside of the range of these forcing frequencies. As the natural frequency tends to increase with stiffness, it is uneconomical to be in the soft-stiff range above 0.93 Hz. It is best to be in the soft-stiff range between 0.31 and 0.42 Hz, however this can be difficult to achieve due to the uncertainty of soil parameters. LeBlanc (2004) suggests that for larger turbines with lower rotation frequencies, the soft-stiff range between 1P and 3P will disappear, and so structures may need to be designed in the soft-soft range. If the natural frequency can be designed below the wave frequency, only inertia-induced responses will dominate. In offshore applications, this is called a 'Compliant Tower', an example of which is the Petronius Platform in the Mexican Gulf.

As prevailing wind directions remain fairly constant, one-way cyclic loading will dominate, leading to an accumulated pile head rotation and deflection, which could damage the above structure. Achmus *et al*. (2009) recommended a value of 10^8 for the number of cycles a typical wind turbine will encounter in its 25 to 30 year lifetime, and a maximum allowable rotation of 0.5 degrees at the pile head. The stiffness of the soil may change with time, and this will also lead to a change in natural frequency that should be designed for.

1.3 Project Objectives

The aims of this research are as follows:

- To investigate the impulse response of a small-scale model monopile at 1-g
- To investigate the harmonic response of a model monopile
- To determine whether a simple model can be used to predict the natural frequency of a model monopile

2 Literature Review

2.1 Lateral Loading of Piles

In its unloaded position, a pile has an equal lateral earth pressure acting on all faces, which depends on the initial state of the soil and the installation method. As the pile is displaced laterally, the pressure on the front side increases and the pressure on the back side decreases, as shown in Figure 2.1.

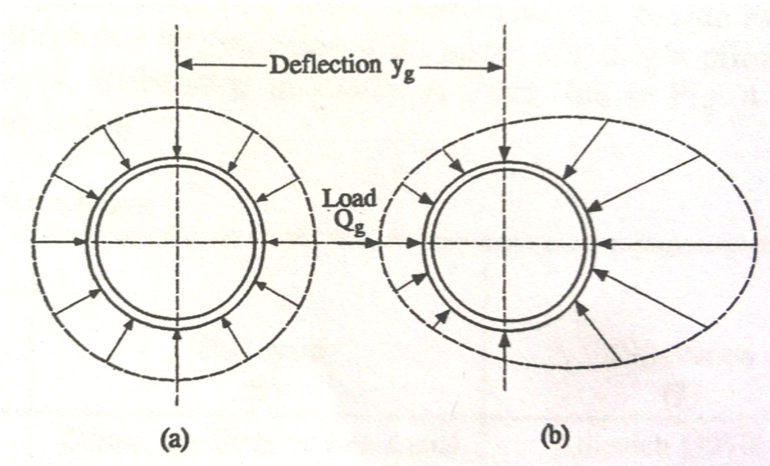

Figure 2.1. Soil reaction distribution around pile. (a) Before lateral loading (b) After lateral loading (Prakash & Kumar, 1996)

Brodbaek *et al*. (2009) describe the Mustang Island tests carried out in 1966, in which two piles of the same diameter in the same sand with an embedded length-to-diameter ratio of 34.4 were tested in seven different load cases. From this, p-y curves were developed for cohesionless soils, which describe the non-linear relationship between the lateral soil resistance per unit length of the pile and the lateral deflection of the pile. Brodbaek describes the formulations of the p-y curves developed by Reese *et al*. (1974), as shown in Figure 2.2.

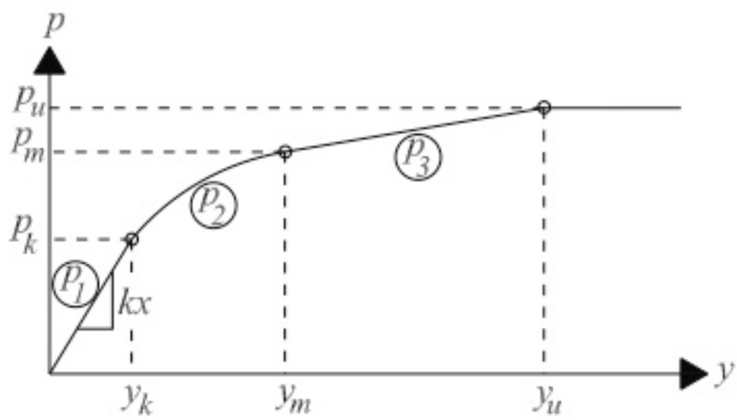

Figure 2.2. Reese's p-y curve produced from Mustang Island tests (Brodbaek *et al*., 2009)

The p-y curve is split into four sections. Expressions are first calculated for p_f, which is dependent only on the internal angle of friction of the sand, the depth, the diameter and the effective unit weight of the soil. These are multiplied by empirical factors to find p_u and p_m. Focusing only on the initial section for small strains, the gradient is *kz*, where *k*, the initial modulus of subgrade reaction, was suggested by Reese *et al*. (1974) to be 5.4 MN/m^3 for loose sand, 16.3 MN/m^3 for medium sand and 34 MN/m^3 for dense sand, and *z* is the depth. The exact derivations of sections 2 to 4 of the graph are less important here.

The design codes adopted by the American Petroleum Institute (API) and subsequently DNV (2010) for offshore wind turbines suggest the use of hyperbolic p-y curves. First the ultimate static resistance is calculated:

$$p_u = \min\left\{(C_1 z + C_2 D)\gamma' z \quad , \quad C_3 D \gamma' z\right\} \tag{2.1}$$

where *D* is the pile diameter, *γ'* is the effective unit weight, and C_1, C_2 and C_3 depend on the friction angle as shown in Figure 2.3.

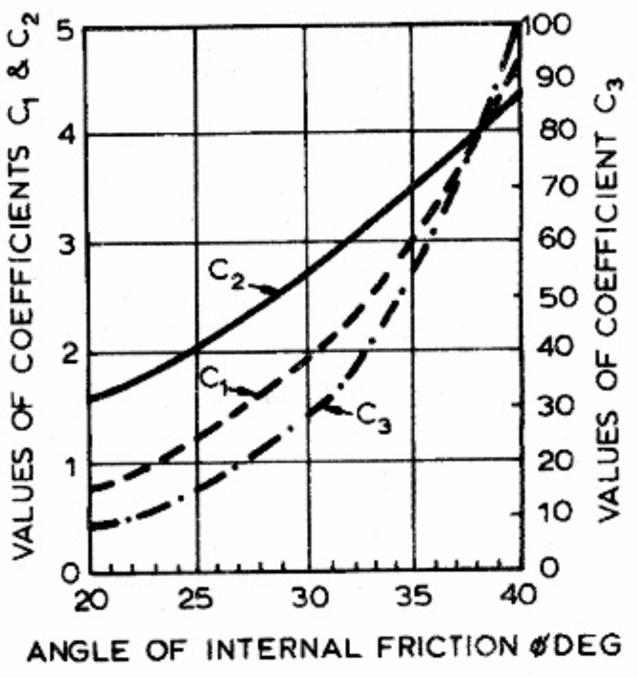

Figure 2.3. C_1, C_2 and C_3 factors suggested by DNV (2010)

Then, the p-y curves are constructed according to:

$$p = A p_u \tanh\left(\frac{kz}{A p_u} y\right) \tag{2.2}$$

where *A* is 0.9 for cyclic loading and $(3 - 0.8z/D) \geq 0.9$ for static loading. The variation in *k* with relative density is shown in Figure 2.4.

For small *y*,

$$p = kzy \tag{2.3}$$

And so, for small strains, Reese's method and the DNV code are the same, provided the same value of *k* is chosen. Brodbaek *et al.* (2009) show that both methods give similar p-y curves. For small pile-head deflections, *k* has the greatest influence on stiffness, whereas for larger pile-head deflections, the angle of friction has a greater influence.

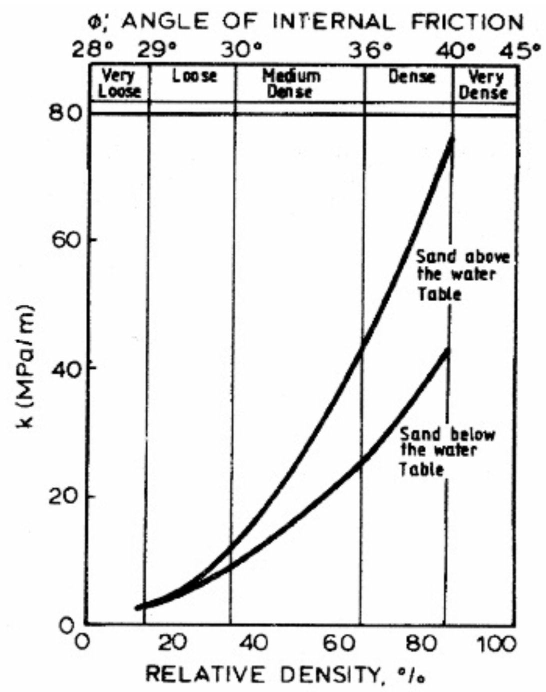

Figure 2.4. Variation of *k* with relative density (DNV, 2010)

Both Brodbaek *et al.* (2009) and Prakash & Kumar (1996) describe the Winkler approach, in which the lateral resistance of the soil is modelled as a series of springs along the length of the pile, each of stiffness *k*, the secant stiffness of the p-y curve which decreases with increased deflection. Although this can be used to model layered soils, it does not take into account shearing between soil layers, and so may be conservative. Continuous models of the beam might aim to solve the equation suggested by LeBlanc *et al*. (2010):

$$E_p I_P \frac{d^4 y}{dz^4} - p(y) = 0 \tag{2.4}$$

However, for short beams the Timoshenko beam theory should be used to take into account shear strains and axial loads, which requires the solution of two differential equations (Brodbaek *et al*., 2009).

Brodbaek *et al*. (2009) argue that it is questionable that the lateral resistance of the pile does not depend on bending stiffness of the pile, as p-y curves should describe the soil-pile interaction. Further, the interaction between vertical and horizontal loads is not considered. At larger displacements there may be a considerable increase in capacity with vertical loads. The initial stiffness of the pile is independent of the diameter, and only a function of the relative density of the sand, an assumption that may not be valid outside the range of the original tests. p-y curves do not take into account the installation method, the initial stress state of the soil (the initial coefficient of earth pressure K_0 is assumed to be 0.4) and the loading regime (LeBlanc *et al*., 2010). However, Achmus *et al*. (2009) argue that the stress changes due to installation of the pile take place in a much smaller area than the soil contributing towards the lateral resistance. Byrne & Houlsby (2003) suggest that the p-y curves be used with care for cyclic loading as they are derived from monotonic load tests, which do not take into account the loading rate and load reversal.

Often the lateral deformation properties of piles are modelled using finite element methods, however the accuracy of these simulations is dependent on the validity of the constitutive soil models used. Due to the non-linear nature of the soil, and the required coupling matrices between solid and fluid phases, many thousands of degrees of freedom can result, meaning that this process is computationally heavy. For dynamic analyses, a method of collecting energy dissipated through the soil at the boundary needs to be considered.

2.2 Monopile Foundations

Monopile foundations are relatively rigid piles, meaning that they rotate without bending considerably, and develop a toe-kick when over-turning (LeBlanc *et al*., 2010). A pile is rigid in the range:

$$4.8 < \frac{E_s L^4}{E_p I_p} < 388.6 \tag{2.5}$$

Where the subscript S denotes soil properties, and the subscript P pile properties. For a diameter of 4 m, a wall thickness of 0.06 m and an embedded length of 18 m, the range of E_s for which the pile is rigid is 14 to 1121 MPa, so a typical monopile will be rigid for most soils. Alderlieste (2011) suggests that the centre of rotation is located at a depth of about 0.8 times the embedded length, hence the ‘toe-kick’ developing at the base in Figure 2.5. This base shear is difficult to express quantitatively. Achmus *et al*. (2009) found that for tests on rigid piles in sandy soils, the pile performance is very much dependent on the embedded length. As the load level increases, the point of rotation moves deeper, meaning that the relationship between pile head rotation and pile head displacement is not fixed.

Alderlieste (2011) found that an increase in the eccentricity of the loading leads to a decrease in the lateral stiffness of the pile.

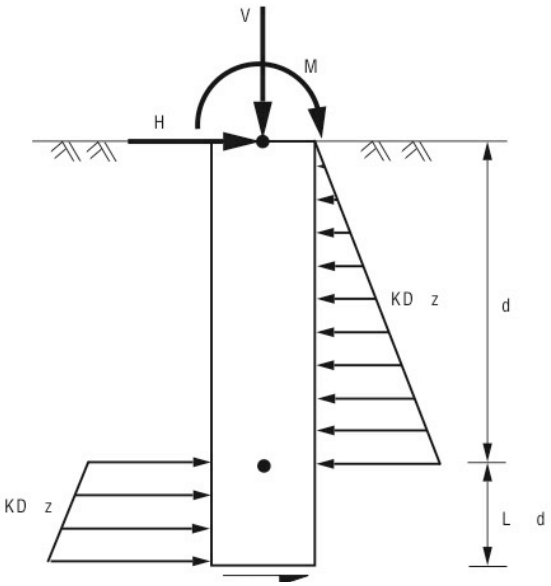

Figure 2.5. Rigid pile with rotation point and toe-kick (LeBlanc *et al*., 2010)

There remains no validated method for the design of offshore rigid monopiles. The DNV (2010) codes based on API standards for oil and gas installations are often adopted. However, LeBlanc *et al*. (2010) argue that these codes are being used outside of their verified range, as the Mustang Island tests on which they were based were carried out on flexible piles of 0.61 m diameter and 21 m length. The same shortcomings of the p-y curves described in section 2.1 still apply, most notably ignoring the shear at the base of the pile, which will be more significant for rigid monopiles. The DNV codes are hence used primarily for the evaluation of the ultimate lateral capacity of the pile. The method does not take into account any changes in stiffness over the structure's lifetime, and accumulated rotation can reduce the resistance of the soil-pile system. The DNV (2010) codes recommend solution of equation 2.4 by use of finite difference methods, but that "caution must be exercised … where the initial slope of the p-y curves may have an impact". Kuhn (2001) suggests that a lateral head deflection in the range of millimetres can be expected for monopiles, and Brodbaek *et al*. (2009) agree that as only small pile head rotations are acceptable, the initial slope of the p-y curve is key. That *k* is independent of the pile diameter in this code is clearly an issue. Alderlieste (2011) found that the p-y curves led to an overestimate of stiffness for pile tests in dry sand in a centrifuge and that the initial stiffness was greater for a larger diameter pile than for a smaller diameter pile. Alderlieste suggests a substitution of *k* in the p-y formula with the stiffness at 50% of the peak load determined from a triaxial test. The diameter issue remains however, and it is clear that more research is required into the initial stiffness of full-scale rigid monopiles.

Cyclic loading for offshore monopiles often occurs in the direction of prevailing winds. Any change in direction will lead to lower accumulated rotations due to multi-directional loading (LeBlanc *et al*., 2010). The worst case to design for is therefore uni-directional cyclic loading. Bhattacharya *et al*. (2010) suggest that cyclic shear strains induced in saturated soil will lead to pore pressure generation, and may alter the foundation stiffness, thus affecting the long-term performance. There is limited documentation of the stiffness changes of a wind turbine monopile over its entire lifetime of 20 to 30 years, but various research has been carried out into the expected stiffness changes with cyclic loading.

Verdure *et al*. (2003) concluded that for centrifuge testing of flexible piles in sand, the secant stiffness was 1.5 to 3 times larger during cyclic loading than in the original monotonic loading and further increased with one-way cyclic loading. Alderlieste (2011) agreed with this for similar tests, with 90% of the extra stiffness gain in the first 20 cycles, and the remaining gain in the next 480 cycles. This result is shown in Figure 2.6, which also shows that the tangent stiffness is around 50% higher than the secant stiffness.

LeBlanc *et al*. (2010) describe the method proposed by Long and Vanneste (1994) for deterioration of the initial p-y curves after this initial gain, with the rate dependent on installation method, soil density and load characteristics. However, this method is based on the results of just 34 tests. Achmus *et al*. (2009) argue that as the p-y curves are based on tests with fewer than 200 cycles, a degradation model should be applied based on finite element analysis and drained cyclic triaxial tests, where the decrease in stiffness is due to an increase in plastic strain.

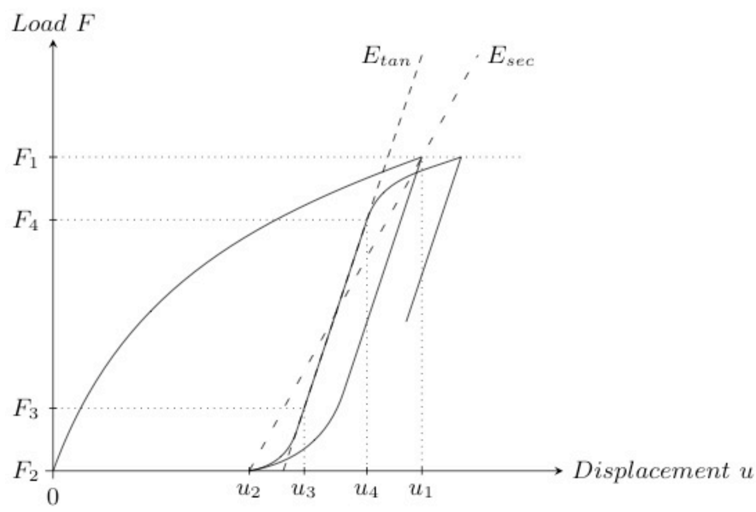

Figure 2.6. Increase in stiffness with one-way cyclic loading (Alderlieste, 2011)

Achmus *et al*. (2009) found from tests on a rigid pile in sandy soils that the entire length was subject to a decrease in soil stiffness during cyclic loading. The rotation accumulation was found to depend on the load level relative to ultimate capacity, which itself depends on the embedded length. This agrees with the work of Bhattacharya *et al*. (2010), who found that the stiffness reduction was greater at a higher strain level. This change was also found to be greater when the forcing frequency was near the natural frequency of the system. Conversely, LeBlanc *et al*. (2010) found an increase in stiffness with cyclic loading for sand of relative density of 4% and 38%. An increase in stiffness may be expected for loose sands, but LeBlanc argues that this is independent of relative density. Clearly more tests are required to validate this. Further, the piles were subjected to only 10^4 cycles, with results extrapolated out to 10^7 cycles.

2.3 Predicting the Natural Frequency of Flexible and Rigid Piles

Kuhn (2001) suggests three different methods for the simple evaluation of the natural frequency of rigid or flexible piles before complex finite element analysis is undertaken, shown in Figure 2.7.

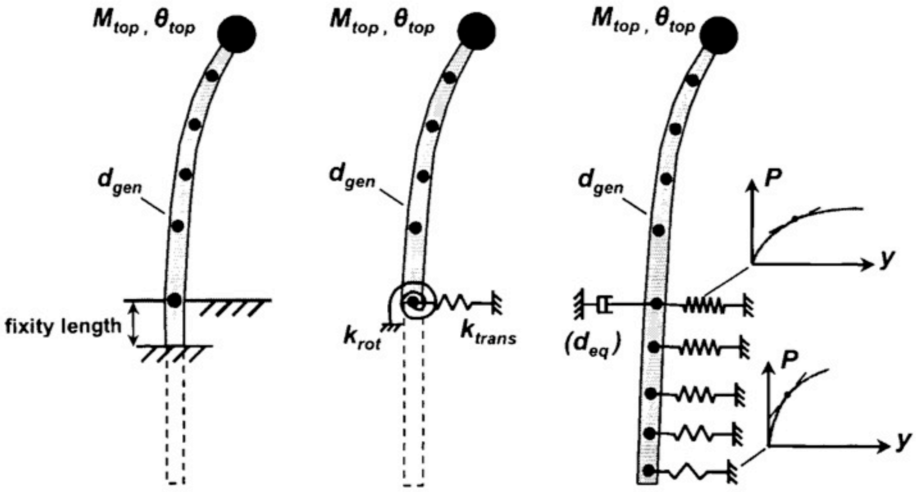

Figure 2.7. Three different methods for evaluating natural frequency of piles (Kuhn, 2001)

The first method involves using an 'apparent fixity length', typically 6 *D* for flexible piles and 3.3 to 3.7 *D* for rigid piles. This is the length below the mudline at which the pile is assumed to be rigidly clamped. The second method has springs representing the rotational and lateral stiffness at the pile head. Randolph (1981) developed expressions for these springs using finite element analysis for flexible piles relating the applied moment and lateral force to the pile head rotation and displacement in terms of pile and soil parameters. Randolph introduces the concept of the critical length of a flexible pile, at which an increase in length does not affect the lateral resistance. The third model uses p-y curves and the Winkler model, with a dashpot representing the soil damping.

Adhikari & Bhattacharya (2012) used Randolph's expressions to predict the natural frequency of wind turbine structures. To measure the stiffness of these equivalent springs experimentally, a static moment test is suggested to find the initial pile head rotational stiffness, and a lateral push over test to find the lateral spring stiffness. Analytical expressions derived from Randolph's results for the springs in Figure 2.7b are:

$$k_{trans} = \frac{k_{rep}}{\sqrt{2}}\left(\frac{L_c}{4}\right) \qquad \left[Nm^{-1}\right] \tag{2.6}$$

$$k_{rot} = \frac{k_{rep}}{\sqrt{2}}\left(\frac{L_c}{4}\right)^3 \qquad \left[Nm\right] \tag{2.7}$$

where k_{rep} is the representative soil stiffness, and L_c is the critical length, given by:

$$k_{rep} \approx 10G\left(\frac{G}{E_P}\right)^{0.14} \qquad \left[Nm^{-2}\right] \tag{2.8}$$

$$L_c = 4\left(\frac{E_P I_P}{4k_{rep}}\right)^{0.25} \qquad \left[m\right] \tag{2.9}$$

For the three wind turbines considered, accuracies of 14% and 16% were achieved for the two with natural frequency data (one an overestimate, one an underestimate). However, the piles are all flexible. For two nearly-rigid piles, the critical length is found to be 95% of the length of the pile. No guidance is given on what to do if this is greater than the length of the pile. Algebraic manipulation shows that this will be the case if:

$$G < E_P\left(\frac{6.4 I_P}{L^4}\right)^{1/1.14} \tag{2.10}$$

Substituting in the second moment of area for a tubular monopile:

$$G < E_P\left(\frac{0.8\pi D^3 t}{L^4}\right)^{1/1.14} \tag{2.11}$$

For a typical steel monopile with E_s=210 GPa, L/D=5 and L/t=100 (Bhattacharya *et al.*, 2010), if the shear modulus of the soil is less than 120 MPa, the critical length will be longer than the pile and so these expressions cannot be used. At Kentish flats, the shear modulus was found to be 80 MPa (Bhattacharya *et al.*, 2010). The calculation of the natural frequency of the system does not appear to take into account the mass of the foundation, which is likely to be comparable to the mass of the tower and the rotor.

The 'zero toe-kick' suggestion of Germanischer Lloyd states that the pile deflection should be zero at two points, to reduce the sensitivity of the pile to cyclic loading (Achmus *et al*., 2009). This is achievable for offshore piles of 2.5 m diameter, but Achmus found that this was an unsuitable criterion for large diameter monopiles, and that it is more efficient to design for allowable accumulated deflection and rotation over its lifetime.

2.4 Experimental Modelling and Dimensional Analysis

Bhattacharya *et al*. (2010) tested a model dural-alloy monopile of diameter 22 mm in clay at 1-g. The frequency and damping of the system was measured by a free vibration test, with the acceleration measured after an initial vibration. LeBlanc *et al*. (2010) carried out tests on a copper monopile of diameter 80 mm in both loose and medium-dense sand at 1-g. They isolated the test rig from external vibrations, and measured the response of piles to long-term cyclic loading at a fixed frequency.

LeBlanc *et al*. (2010) suggest the following dimensionless groups on applied loads, moments, and dimensions:

$$\left[\frac{M}{L^3D\gamma'}\right] \quad , \quad \left[\frac{H}{L^2D\gamma'}\right] \quad , \quad \left[\frac{V}{L^2D\gamma'}\right] \quad , \quad \left[\frac{M}{HL}\right] \quad , \quad \left[\frac{L}{D}\right]$$

Bhattacharya *et al*. (2010) suggest a further dimensionless group of to keep the strain level in the soil similar:

$$\left[\frac{H}{GD^2}\right]$$

The denominator explains why large diameter piles are used to reduce the strain level in the soil. Small-scale saturated tests can be difficult to carry out as Bhattacharya *et al*. (2010) argue that the ratio of forcing frequency to natural frequency should be kept the same, while also maintaining the former such that pore pressure generation is similar. LeBlanc *et al*. (2010) argue that tests in sand are likely to be fully drained, and so tests can be carried out on dry sand, taking into account differences in effective unit weights.

2.5 Conclusions

This literature review has introduced the origins and limitations of p-y curves for the design of monopiles. It is clear that the effect of pile diameter on the initial lateral stiffness needs to be further investigated. Current simple models for evaluating the natural frequency of rigid piles are limited, and the initial lateral stiffness is important at the low strain levels expected. Dimensionless groups have been suggested for small-scale modelling of the problem.

3 Experimental Methods

Experiments were carried out at the Schofield Centre, University of Cambridge.

3.1 Experimental Setup

It was decided that tests should be carried out on small-scale model monopiles at 1-g, the time constraints of the project meant that centrifuge testing was unfeasible. A standard tub of 850 mm diameter and 400 mm depth was used. Measured and calculated model monopile properties are shown in Table 3.1.

Table 3.1. Properties of Aluminium Model Monopile

Length (mm)	450
Diameter (mm)	76
Wall thickness (mm)	1.7
Mass (kg)	0.463
E (GPa)	69
I_{xx} (mm^4)	2.74×10^5

The first stage is to check the rigidity of the pile using equation 2.5. This model pile will be rigid provided the average soil stiffness E_s is in the range of 7.7 to 619.5 MPa, using an embedded depth L of 0.33 m. The stiffness is likely to be towards the lower end of this range, corresponding to very rigid. Similarly, the equations for calculating the stiffness of a flexible pile presented in Section 2.3 are only valid for G greater than 32 MPa, using equation 2.11, which is unlikely to be the case. The dimensionless groups for the model monopile are compared with typical values in Table 3.2. As only cyclic lateral loading is considered, the vertical loading on the pile is not taken into account. The embedded length of the model pile L was chosen to be 0.33 m, due to the depth of the tub. This gives a slightly smaller L/D ratio than required. The result of the dimensional analysis is that the horizontal loading applied should be ±7.4 N at an eccentricity of 0.13 m. Figure 3.1 shows the monopile in its three different configurations for testing, which will be explained in detail later.

Table 3.2. Dimensional Analysis for the Model Monopile

Dimensionless Group	Typical value	Model monopile	Required parameter
$\frac{H}{L^2 D\gamma'}$	$\frac{\pm 2\times 10^6}{25^2\times 5\times 10\times 10^3} = \pm 0.064$	$\frac{H}{0.33^2\times 0.076\times 14\times 10^3}$	$H = \pm 7.4N$
$\frac{M}{L^3 D\gamma'}$	$\frac{\pm 20\times 10^6}{25^3\times 5\times 10\times 10^3} = \pm 0.0256$	$\frac{He}{0.33^3\times 0.076\times 14\times 10^3}$	$e = 0.13m$
M/HL	0.40	0.39	/
L/D	5.0	4.3	/

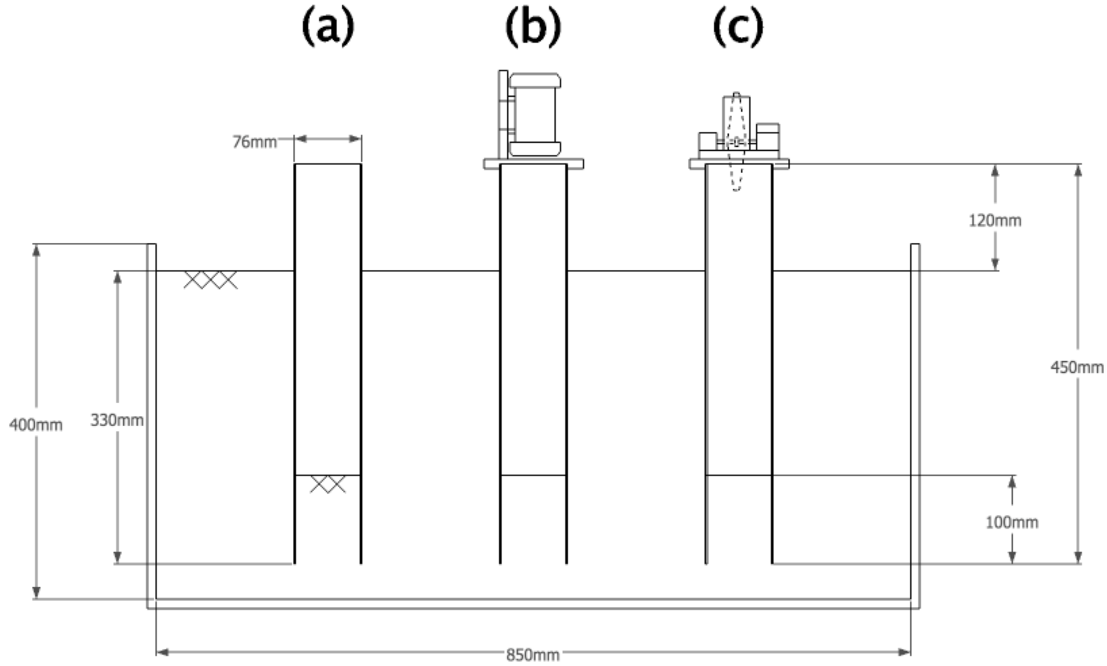

Figure 3.1. Graphic of the three monopile configurations (a) Monopile only (b) Eccentric mass vibrator (c) Piezo-electric actuator

3.2 Soil

The majority of the tests were carried out in Hostun sand, which is often used in research due to its uniformity (Pairaudeau, 2011). The properties of Hostun are listed in Table 3.3 from Mitrani (2006). It was decided that tests should be carried out in dry sand, using the arguments of section 2.4.

Table 3.3. Properties of Hostun sand (Mitrani, 2006)

ϕ_{crit}	33^o
e_{min}	0.555
e_{max}	1.010
G_s	2.65

For later tests, saturated Kaolin clay was used, which had been preconsolidated to 25 kPa, with an expected homogenous shear strength profile. A large vane measured the undrained shear strength s_u to be 10 to 11 kPa at various depths. A smaller vane, believed to be more accurate, consistently measured s_u to be 18 kPa near the surface. A conservative estimate is therefore 15 kPa.

3.3 Impulse Response

Tests were carried out to find the impulse response of the monopile. The impulse was typically applied to the top of the pile using a metal coin. The time trace recorded from accelerometers (described in Section 3.5) was immediately checked for the quality of the impulse applied. Initial tests were carried out on the pile as a cantilever, clamped at the base, as shown in Figure 3.2. This was to investigate any fundamental frequencies of the pile.

Figure 3.2. Monopile clamped at base for cantilever testing

The sand density, embedment depth and impulse application point were recorded for each impulse test in sand. Early tests were carried out on the pile only. Later tests had the added mass of the eccentric mass vibrator (EMV) or the base plate at the top. A summary of all embedded impulse tests is given in Table 3.4.

Table 3.4. Summary of Embedded Monopile Impulse Tests

Test numbers	Embedment Depth (mm)	Upper Accelerometer	Lower Accelerometer	Added mass on top
Loose sand tests				
I-L-1 - I-L-7	340	35g	35g	/
I-L-8 - I-L-11	330	35g	1.7g	/
I-L-12 - I-L-14	330	35g	1.7g	EMV
I-L-15 - I-L-17	330	35g	1.7g	/
I-L-18 - I-L-20	330	35g	1.7g	EMV
I-L-21 - I-L-24	330	1.7g	1.7g	/
I-L-25 - I-L-28	330	1.7g	1.7g	EMV
I-L-29 - I-L-34	330	1.7g	1.7g	Base plate
Dense sand tests				
I-D-1 - I-D-9	330	1.7g	1.7g	Base plate
I-D-10 - I-D-15	185	1.7g	1.7g	Base plate

3.4 Harmonic Response

3.4.1 Eccentric Mass Vibrator

The Vibratéchniques Ltd. eccentric mass vibrator (EMV) used is shown in Figure 3.3, attached to the base plate at the top of the monopile. It consists of an A. C. motor, to which pairs of moon-shaped discs, each of mass 6 grams, are added. One disc must be added either side of the motor to prevent a couple from being generated. When rotating at 50 Hz, the discs act as out-of balance masses to produce a harmonic force of amplitude 10.8 N per pair, acting in all directions within a horizontal plane. A maximum of eight discs (43.2 N) can be added. The total mass of the EMV and the base plate is 1.54 kg. Unfortunately, no method of controlling the frequency of the EMV was found, so instead tests were carried out in loose sand whereby the response of the pile was measured after the EMV was either switched off or switched on, with the hope of finding frequencies in the range of 0 to 50 Hz.

Figure 3.3. Eccentric mass vibrator

3.4.2 Piezo-electric Actuator

A Cedrat Technologies APA400MML piezo-electric actuator was attached to the base plate as shown in Figure 3.4. A signal generator was used to produce a sinusoidal signal of known frequency, which was then amplified by 20 times using the amplifier. The signal generator was set to an offset of 3 V, with a maximum allowed amplitude of 6 V peak-to-peak to conform with the maximum actuator range of -20 to 140 V.

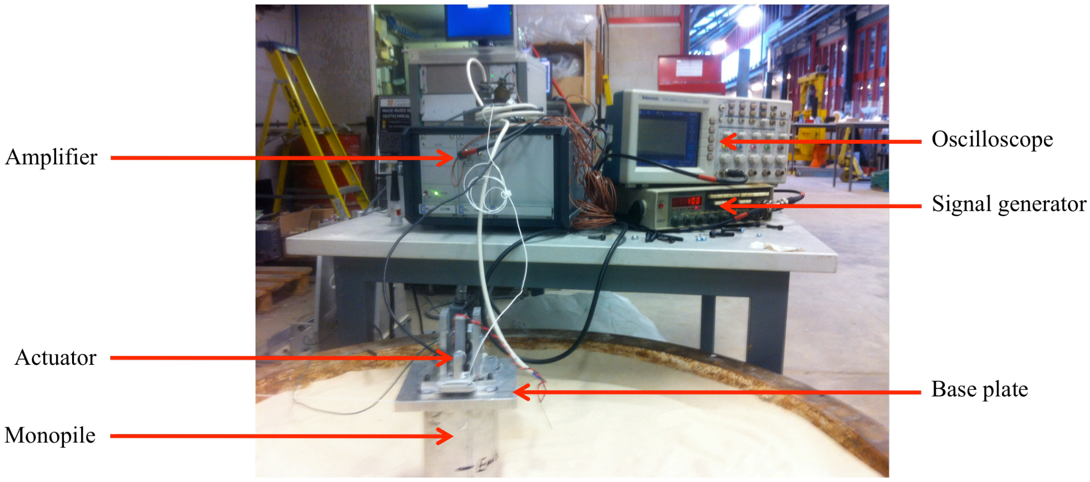

Figure 3.4. Piezo-electric actuator attached to monopile

The voltage applied to the piezo-electric crystal causes it to expand and contract vertically. The frame which restrains it therefore expands and contracts horizontally, loading the top of the pile cyclically in two directions. An increase in applied voltage gives an increase in force. The masses of the base plate and actuator were measured to be 0.272 kg and 0.374 kg respectively.

Initial tests were again carried out on the pile as a cantilever, followed by tests in loose sand at an embedment of 330 mm (Figure 3.5a). The voltage amplitude was kept constant and the response of the pile recorded in 5 second samples at set frequencies. These tests were carried out using different voltage amplitudes to investigate the effect of force on the natural frequency. Similar tests were carried out in clay of depth 200 mm, with an embedment of 185 mm as shown in Figure 3.5b. These tests could be compared with tests I-D-10 to I-D-15 in dense sand. A summary of all piezo-electric actuator tests is given in Table 3.5, all using two 1.7 g accelerometers. The order the tests were performed in is important as stiffness changes may have occurred due to cyclic loading. Unfortunately, the piezo-electric actuator broke before tests could be carried out in dense sand, and the replacement was not scheduled to arrive before testing was completed.

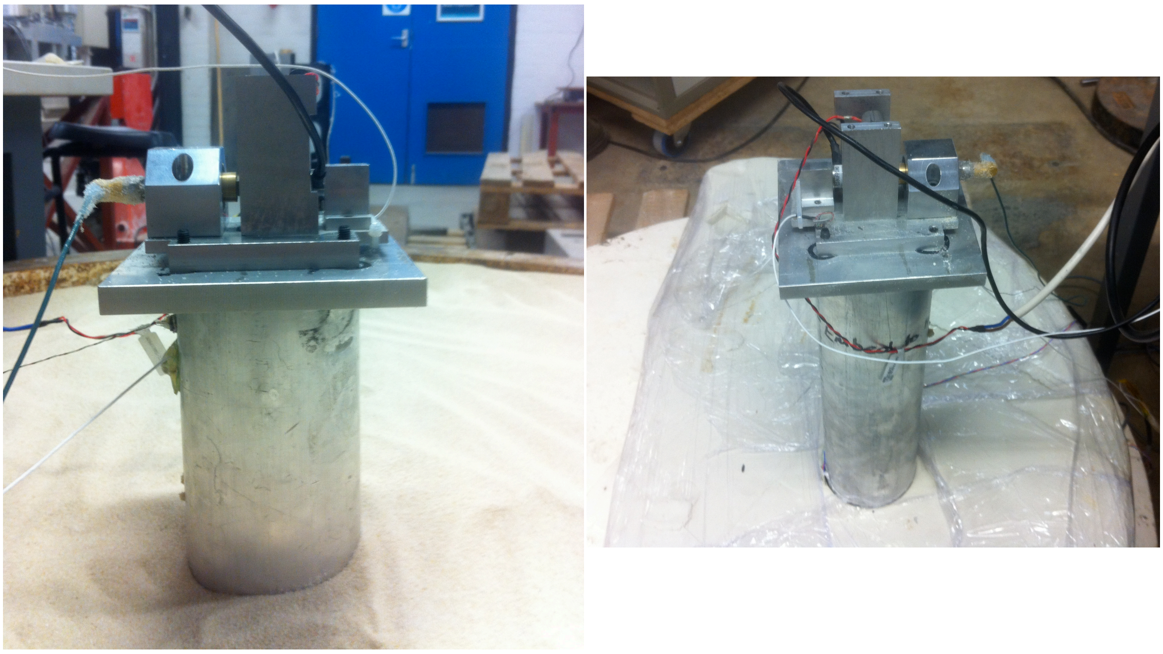

(a) (b)

Figure 3.5. Harmonic tests using piezo-electric actuator. (a) In loose sand (b) In clay

Table 3.5. Summary of Piezo-Electric Actuator Tests

Test Numbers	Frequency Range	Signal Amplitude (p-p, V)
Cantilever Tests		
H-1 - H-39	13-110 Hz @ 1-5 Hz intervals	6
Sand Tests		
H-L-1 - H-L-18	15-100 Hz @ 5 Hz	6
H-L-19 - H-L-30	70-95 Hz @ 5 Hz	3
H-L-31 - H-L-48	15-100 Hz @ 5 Hz	4.5
H-L-49 - H-L-64	80-95 Hz @ 1 Hz	4.5
H-L-65 - H-L-80	15-30 Hz @ 1 Hz	4.5
H-L-81 - H-L-94	80-93 Hz @ 1 Hz	6
H-L-95 - H-L-104	13-22 Hz @ 1 Hz	6
Clay Tests		
H-C-1 - H-C-14	12-25 Hz @ 1 Hz	6
H-C-15 - H-C-29	30-100 Hz @ 5 Hz	6
H-C-30 - H-C-41	86-99 Hz @ 1 Hz	6
H-C-42 - H-C-44	26-28 Hz @ 1 Hz	6
H-C-45 - H-C-62	63-84 Hz @ 1 Hz	6
H-C-63 - H-C-75	15-28 Hz @ 1 Hz	4.5
H-C-76 - H-C-92	30-110 Hz @ 5 Hz	4.5
H-C-93 - H-C-103	91-103 Hz @ 1 Hz	4.5
H-C-104 - H-C-114	31-43 Hz @ 1 Hz	4.5
H-C-115 - H-C-132	67-89 Hz @ 1 Hz	4.5
H-C-133 - H-C-141	102-110 Hz @ 1 Hz	4.5

3.5 Instrumentation, Measurement and Analysis

The acceleration of the pile was primarily measured using Micro-Electro-Mechanical Systems (MEMS) sensors. In total, two 1.7 g accelerometers and two 35 g accelerometers were used. The 'upper' accelerometers were attached 10 and 30 mm from the top of the pile, and the 'lower' accelerometers 190 mm from the base, on the opposite side to the upper accelerometers, as shown in Figure 3.6. The manufacturer (Analog Devices) calibrations and frequency ranges for the accelerometers are shown in Table 3.6. A piezo accelerometer was used to measure the force applied by the piezo-electric actuator, with a calibration of 6 g/V. As the mass of the piezo crystal is 0.0475 kg, this becomes 2.8 N/V.

Table 3.6. Accelerometer Calibrations

	35 g (ADXL78)	1.7 g (ADXL103)
Sensitivity (mV/g)	55	1000
Typical Bandwidth (Hz)	400	2500

A 5 V power supply was provided to the accelerometers, which in turn output 2.5 V at zero acceleration. The output of the accelerometers was recorded in DasyLab 8.0, using a sampling rate of 20 kHz. Data was then analysed using MatLab, using the following steps:

- Import data and select range of interest
- Subtract overall mean value from all data to remove D.C. offset
- Use the *fft* (Fast Fourier Transform) function *fft(data, length of signal to nearest power of 2)*
- Multiply each value by its conjugate to remove complex components

For an impulse or step response there is a trade-off between using a longer sample, which increases the frequency resolution of the Fourier transform, and a shorter sample, which will have less noise after the signal has died down. The frequency resolution is:

$$\frac{f_{\text{sampling}}}{\text{Length of signal (nearest power of 2)}} \tag{3.1}$$

Decreasing the sampling frequency reduces the length of signal by an equivalent amount so does not resolve the problem. A solution is to increase the sensitivity of the accelerometers.

3.6 Experimental Setup

For the piles installed to an embedment of 330 mm, it was decided pile driving was not suitable, as it might damage the accelerometers on the side of the pile. Instead, the tub was filled to a height of around 130 mm by pouring at a fast flow rate from a low height, to achieve low sand density. At this point, the pile was installed (Figure 3.7), such that a plug of height 100 mm existed inside the pile. The total height of the sand, and the mass of the tub with and without the sand were measured.

(a) (b)

Figure 3.6. Accelerometer locations. (a) Upper accelerometers (b) Lower accelerometers

Figure 3.7. Pile installation in process

To achieve the dense sand state, the tub was subjected to vibration (Figure 3.8), with the reduction in height measured. During vibration, the pile was pushed down to keep the embedment depth at 330 mm. Using the measured heights and masses, and the values for Hostun sand in Section 3.2, the properties for listed in Table 3.7 were calculated.

Table 3.7. Calculated Properties of Loose and Dense Sand

	Loose Sand	Dense Sand
Relative Density I_D	0.29	0.60
Unit Weight γ' (kN/m^3)	13.8	15.1

Figure 3.8. Vibration of sand

For the clay sample, the only option was to install the clay by driving, so the monopile was pushed in slowly to an embedment of 185 mm, such that the lower accelerometer was above the clay surface. For a consistent comparison, the monopile for the equivalent test in dense sand was driven in to the same embedment.

4 Model for Predicting the Natural Frequency

A basic model for predicting the natural frequency of the monopile is shown in Figure 4.1. The system is reduced to a single degree of freedom system with a single spring representing the spring stiffness at the mud level. The mode shape for the first natural frequency is assumed to be a rotation about a depth z_{crit}, which ignores the flexural stiffness of the pile. This model also ignores higher modes of vibration.

This model will consider only the initial stiffness of the p-y curves. *k* values of 9.8 MPa/m and 37.9 MPa/m were found from the DNV (2010) guidelines for loose and dense states respectively. If the soil is split into 33 elements, each of length 10 mm, the sum of the force contributions for the assumed mode shape is:

$$F_{top} = 0.01\sum_{i=1}^{33} kz_i y_i = 0.01k\sum_{i=1}^{33} z_i y_{top}\left(1 - \frac{z_i}{z_{crit}}\right) \tag{4.1}$$

And therefore the equivalent soil stiffness K_{soil} is equal to:

$$K_{soil} = 0.01k\sum_{i=1}^{33} z_i\left(1 - \frac{z_i}{z_{crit}}\right) \tag{4.2}$$

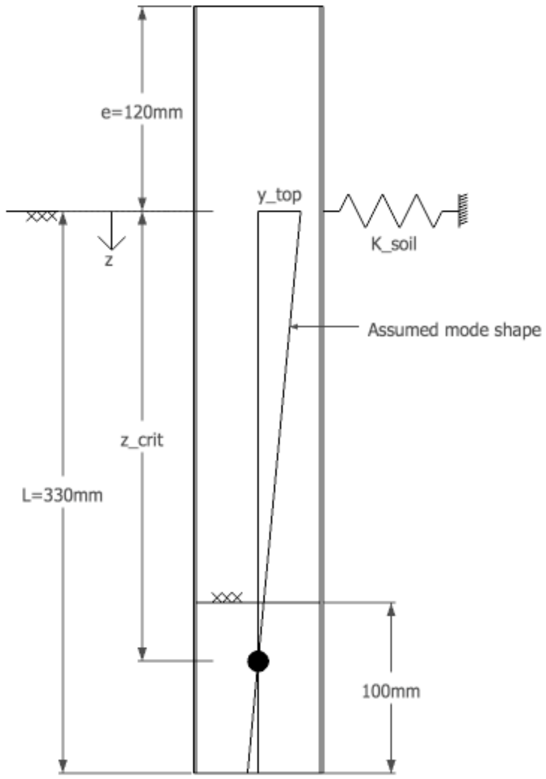

Figure 4.1. Model For estimation of first natural frequency

The moment of inertia of the pile about the rotation point is given by:

$$I = \frac{mL^2}{3} + m\left(e + z_{crit} - \frac{L}{2}\right)^2 \tag{4.3}$$

Both the rotation of the pile θ and the displacement at the centre of gravity y_g can be expressed in terms of the top displacement:

$$\theta = \frac{y_{top}}{z_{crit}} \tag{4.4}$$

$$y_g = \frac{y_{top}\left(1 - \left(\frac{L}{2} - e\right)\right)}{z_{crit}} \tag{4.5}$$

The equivalent mass of the one degree of freedom system is then:

$$M_{eq} = \left(\frac{mL^2}{3} + m\left(e + z_{crit} - L/2\right)^2\right) / z_{crit}{}^2 + m\left(1 - (L/2 - e)/z_{crit}\right)^2 \tag{4.6}$$

The natural frequency of the system is given by:

$$f_n = \frac{1}{2\pi}\sqrt{\frac{K_{soil}}{M_{eq}}} \tag{4.7}$$

In order to find z_{crit}, eccentricity requirements must be considered. e is given by:

$$e = \frac{\sum M_i}{\sum F_i} = \frac{0.01ky_{top}\sum z_i{}^2(1 - z_i/z_{crit})}{0.01ky_{top}\sum z_i(1 - z_i/z_{crit})} = \frac{\sum z_i{}^2(1 - z_i/z_{crit})}{\sum z_i(1 - z_i/z_{crit})} \tag{4.8}$$

Figure 4.2 shows how K_{soil} , M_{eq} , f_n and e vary with the ratio z_{crit}/L for this monopile. The eccentricity and equivalent mass are independent of the soil stiffness. For an eccentricity of 0.12 m, a z_{crit}/L ratio of 0.86 is required, which agrees well with the literature value of 0.80. This gives a natural frequency of 63 Hz for loose sand, and 123 Hz for dense sand. As the eccentricity is increased, these frequencies increase to a maximum of 79 Hz and 156 Hz respectively. The effect of the added mass and inertia of the soil plug of height 100 mm and unit weight 14 kN/m^3 is shown in Figure 4.2. As the plug is at the base of the pile, the displacements are small for z_{crit} larger than 0.7, so the effect is minimal on the natural frequency. Finally, the effect of adding the EMV to the monopile in loose sand is to reduce the natural frequency to 28 Hz.

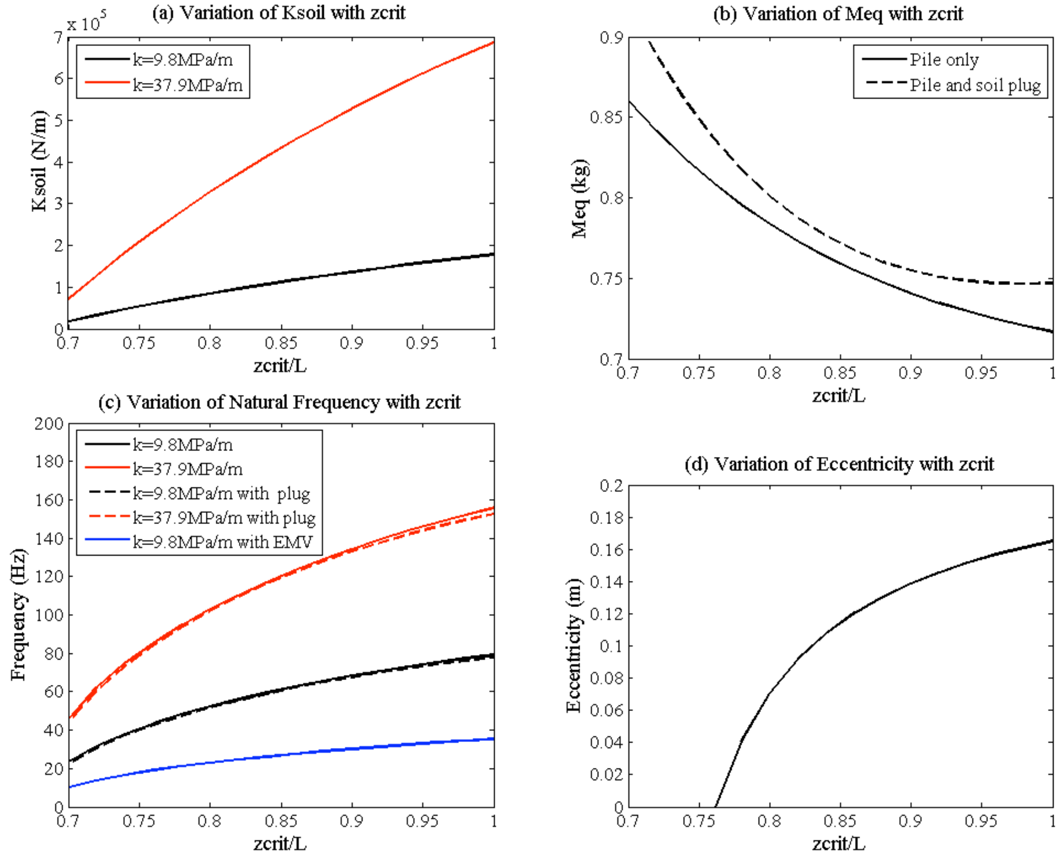

Figure 4.2. Results of Model for 330 mm Embedment

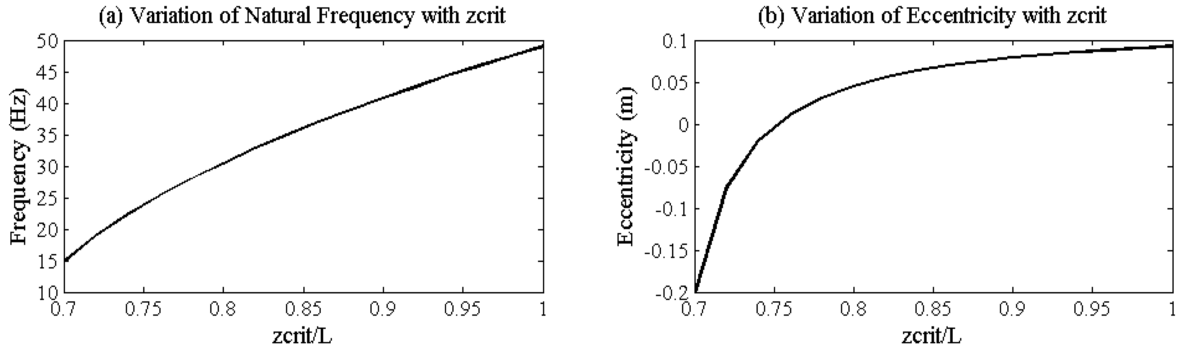

Figure 4.3. Results of Model for 185 mm Embedment in Dense Sand

For the reduced embedment (185 mm) tests in dense sand, Figure 4.3 shows that the predicted frequency varies between 15 and 49 Hz, but the required eccentricity of 265 mm cannot be reached. The resulting mode is likely to involve a coupling of rotation and horizontal modes. The horizontal translational mode consists of a uniform displacement along the length of the pile, with the natural frequency given by:

$$f_n = \frac{1}{2\pi}\sqrt{\frac{kL^2}{2m_{total}}} \tag{4.9}$$

For tests in sand with an embedment of 185 mm, and including the mass of the base plate and soil plug of height 185 mm, the natural frequency is predicted to be 93 Hz.

A clear limitation of this model is that it only considers the initial stiffness, with which caution should be used. k varies significantly with relative density, so the values used may be incorrect. The soil stiffness is actually non-linear, and the depth of z_{crit} is likely to be a function of both force and eccentricity. This model does not take into account the shear force due to the toe-kick at the base of the pile; this is expected to increase the moment and reduce z_{crit} and the natural frequency for a given eccentricity. Finally, the damping of the pile-soil system is not considered, but as this is low it is unlikely to significantly affect the natural frequency.

5 Impulse Response

5.1 Cantilever Tests

An example time trace of a cantilever test is shown in Figure 5.1. The impulse is seen to excite many of the higher frequencies of the cantilever, however peaks of lower frequency components are hidden within the signal. For low levels of damping, the damping ratio is defined as:

$$\zeta = \frac{1}{2\pi}\ln\left(\frac{y_1}{y_2}\right) \tag{5.1}$$

Where y_1/y_2 is the ratio between the amplitude of successive peaks. The damping here is found to be about 6.7%.

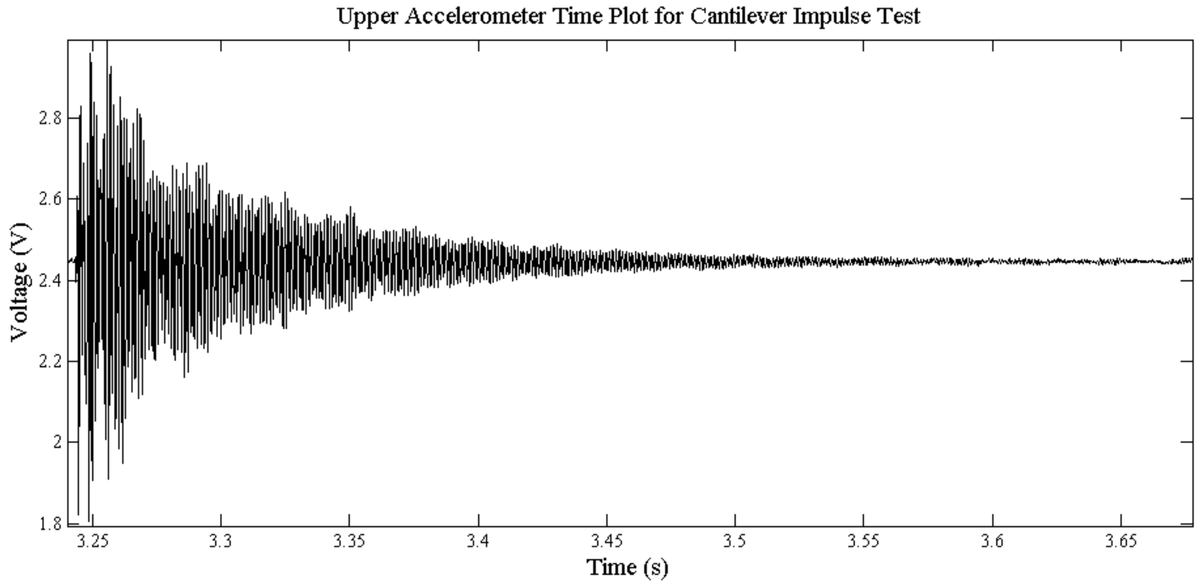

Figure 5.1. Example Time Plot for Cantilever Test Measured by Upper Accelerometer

The cantilever tests were carried out to find any natural frequencies of the monopile itself in the range of interest, which is later shown to be between 0 and 200 Hz. Figure 5.2 shows the Fourier transform for the upper accelerometer for a range of cantilever tests using a sample length of 0.5 seconds. Two tests were carried out with the mass of the actuator and the base plate at the top, with different clamping forces at the base. A third test was carried out with just the mass of the base plate at the top.

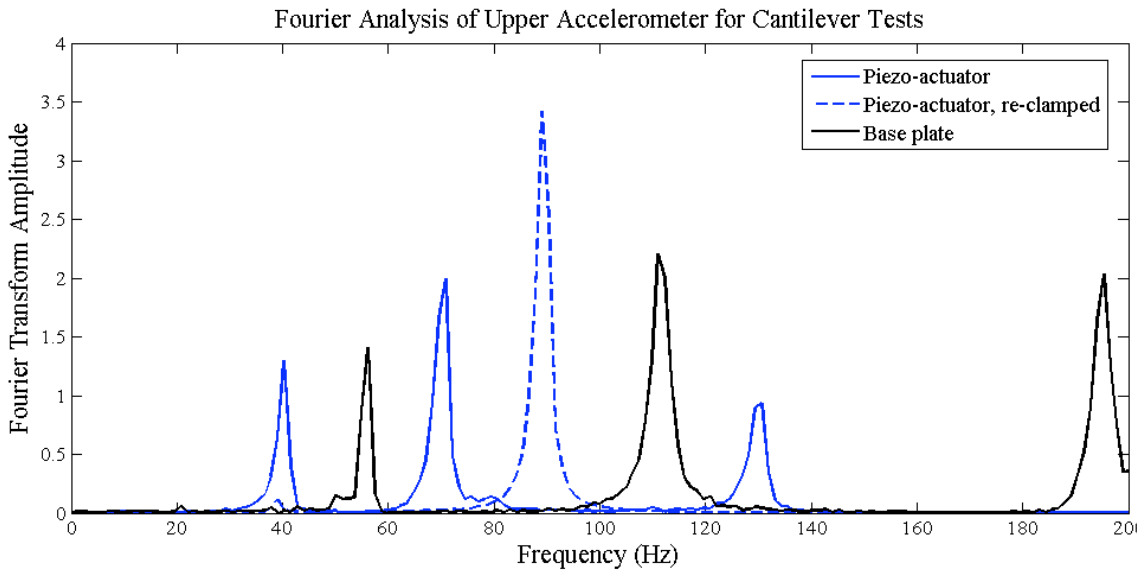

Figure 5.2. Fourier Analysis of Upper Accelerometer for Various Cantilever Tests

Adhikari & Bhattacharya (2012) give the flexural natural frequency of a cantilever with added mass at the top to be:

$$f_n = \frac{1}{2\pi}\sqrt{\frac{3.04E_P I_P}{(m_{top} + 0.227m)L^3}} \tag{5.2}$$

Where m is the mass of the cantilever, and m_{top} is the added mass at the top. For the monopile used, with the added mass of the base plate (0.272 kg), f_1 is 206 Hz. With the added mass of the base plate and actuator (0.646 kg), f_1 is 146 Hz. Peaks at just below these frequencies can be seen for their relevant tests in Figure 4.2. The modes of vibration of the pile are highly complex and unlikely to be orthogonal; the lower frequency peaks are assumed to correspond to contraction and expansion modes of the pile in a horizontal plane. The lower peak only depends on the mass at the top of the pile, whereas the second peak depends on both the added mass and the degree of fixity at the base. A Fourier analysis of the lower accelerometer shown in Figure 5.3 picks up only this lower frequency for all tests. Therefore, when analysing the natural frequency of the embedded pile, frequencies picked up by the lower accelerometer should be analysed first, then possible natural frequencies found can be confirmed by the upper accelerometer.

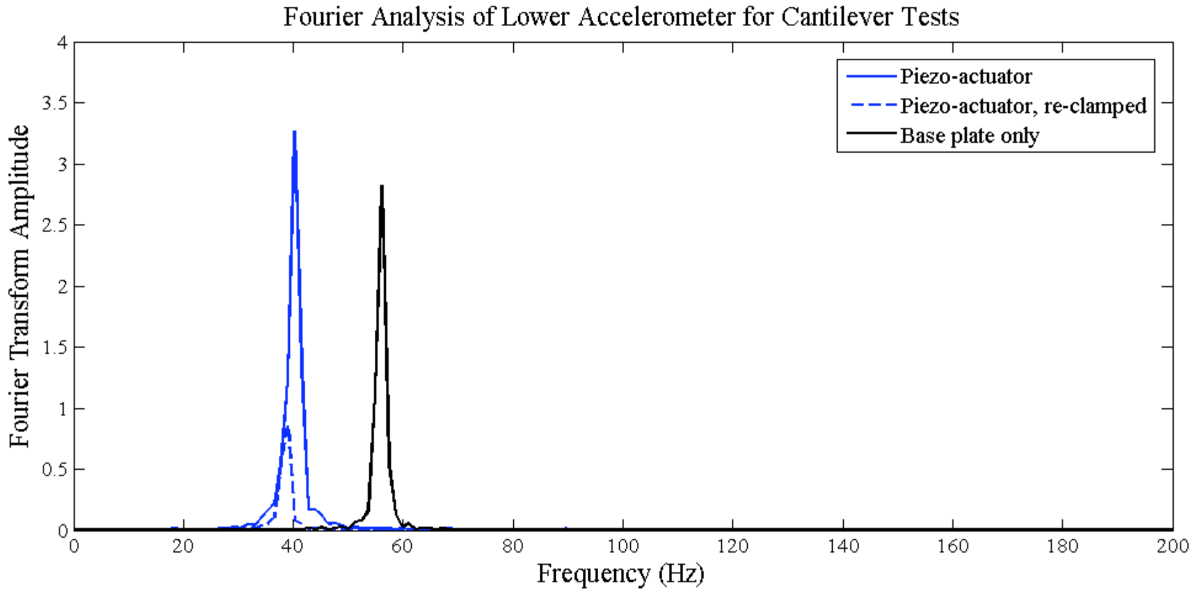

Figure 5.3. Fourier Analysis of Lower Accelerometer for Various Cantilever Tests

5.2 Loose Sand

The first impulse tests (I-L-1 to I-L-7) measured the acceleration using 35g accelerometers. Example time plots for the upper and lower accelerometers are shown in Figure 5.4. Once again, higher frequency components are excited, and the signal dies away very quickly. A Fourier analysis of the signals over a 0.2 second period, corresponding to a frequency resolution of 4.88 Hz, is shown in Figure 5.5. The upper accelerometer appears to give a natural frequency of around 107 Hz. However, as mentioned in section 5.1, it is best to find the natural frequency from the lower accelerometer, which shows mostly noise. A summary of these initial tests is given in Table 5.1, a slash indicates that the Fourier analysis was unclear.

Table 5.1. Possible natural frequencies found by Fourier Analysis

Test number	Upper Accelerometer Peak (Hz)	Lower Accelerometer Peak (Hz)
I-L-1	103	/
I-L-2	/	/
I-L-3	107	/
I-L-4	103	/
I-L-5	/	/
I-L-6	107	/
I-L-7	/	/

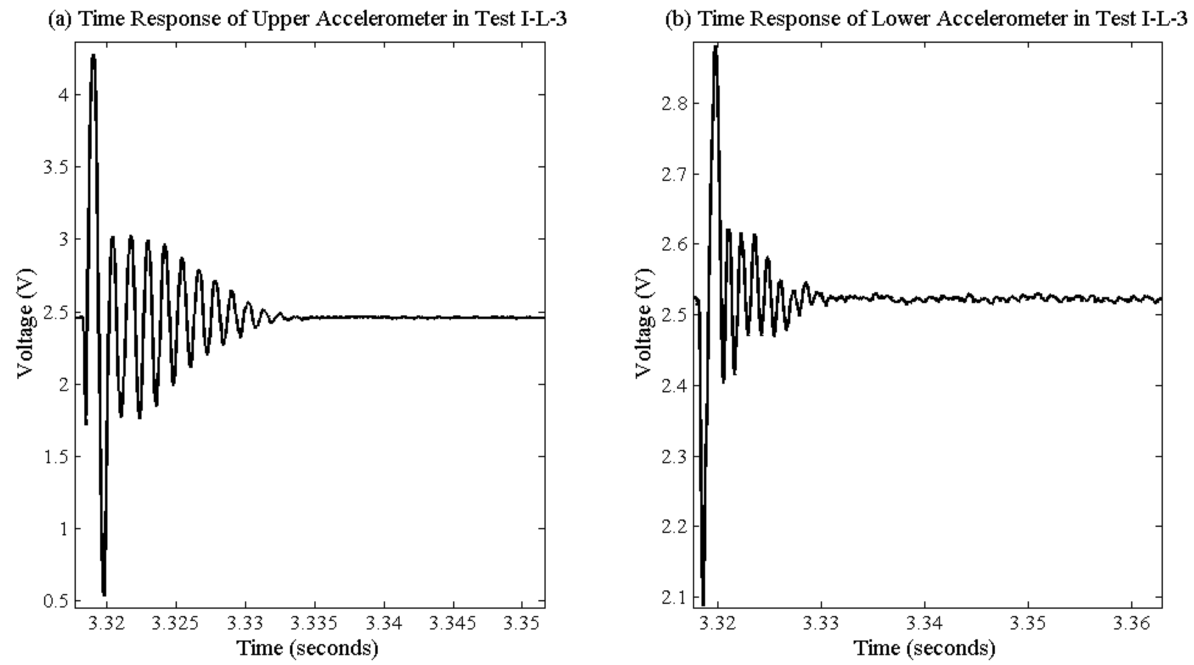

Figure 5.4. Example Time Plots for Tests in Loose Sand using 35g Accelerometers

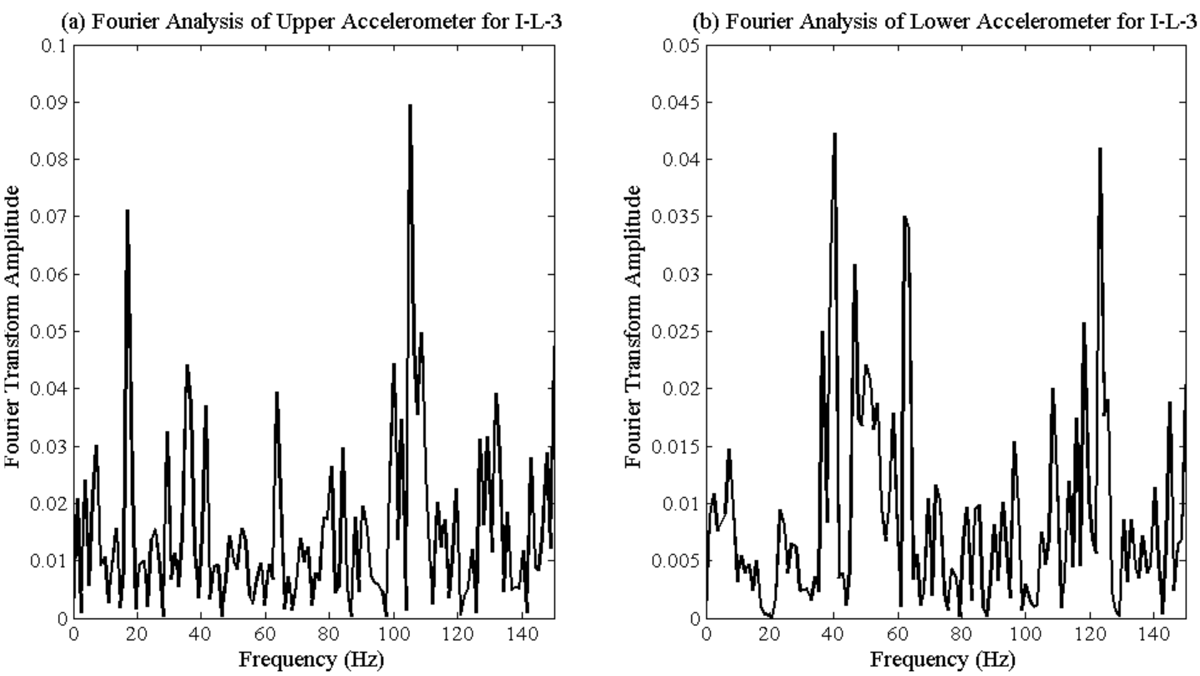

Figure 5.5. Example Fourier Analyses for Tests in Loose Sand using 35g Accelerometers

The decision was made to use the more sensitive lower accelerometer so that a longer sample length could be used to give a better frequency resolution in the Fourier analysis. Figure 5.6 shows an example time trace for an impulse test. An oscillating signal at 50 Hz exists before and after the impulse is applied, suggesting the power supply was not correctly isolated. This problem persisted for tests I-L-8 to I-L-28. Figure 5.7 shows example Fourier transforms for three different tests with a sample length of 0.5 seconds, corresponding to a frequency resolution of 1.22 Hz.

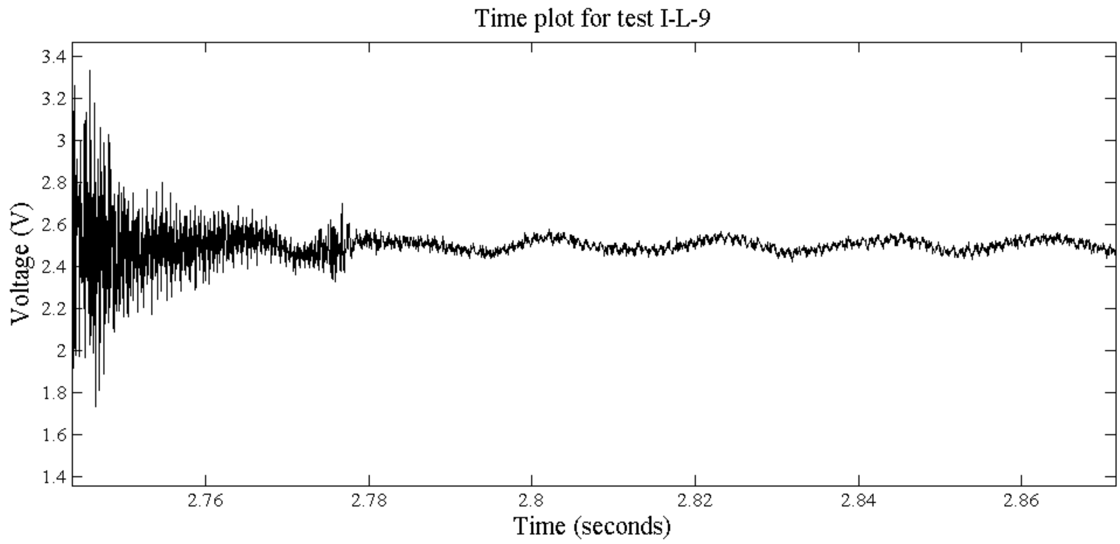

Figure 5.6. Example Time Plot for Impulse Tests in Loose Sand Measured using Lower 1.7g Accelerometer

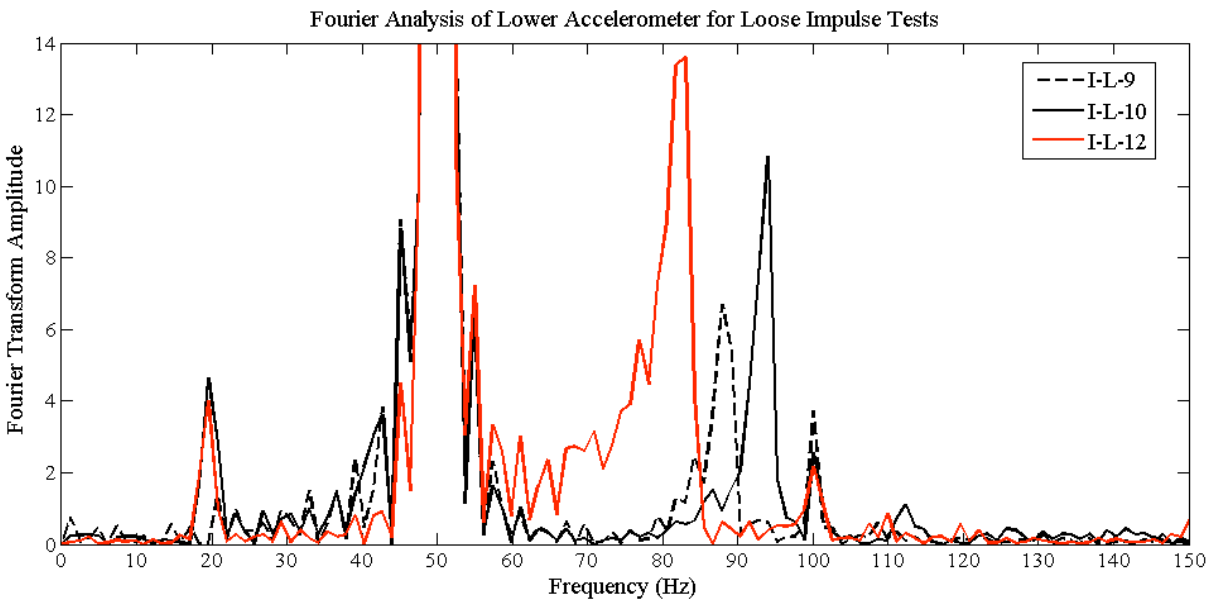

Figure 5.7. Fourier Analyses of Lower 1.7g Accelerometer for Different Impulse Tests

Although the noise frequency at 50 Hz dominates, with a harmonic at 100 Hz, peaks at around 20 Hz and 80 to 95 Hz can be seen. Test I-L-9 was carried out without the EMV on top, and gives a natural frequency of 89 Hz. Cyclic loads of amplitude 21.6 N at 50 Hz were than applied using the EMV for around 2 minutes, corresponding to around 6000 cycles. A similar test, I-L-10, was carried out after these cycles, giving a natural frequency of 94 Hz. In test I-L-12, the extra mass of the EMV was added to the top of the monopile, giving a natural frequency of 82 Hz. The lower peak at 20 Hz remains relatively unchanged throughout, and later tests show that this frequency changes when the tub is moved, suggesting it is a natural frequency of the soil-tub system.

Given that frequency is proportional to $\sqrt{k/m}$, the initial gain in frequency of 5.6% corresponds to an increase in stiffness of 11.6%. This agrees with literature suggesting an initial gain in stiffness over the first 500 cycles. The added mass is expected to reduce the natural frequency, however this is partly counteracted by a gain in stiffness. For a similar magnitude of impulse applied, the displacement is reduced by conservation of momentum. As the stiffness of soil is expected to decrease with an increase in displacement, the extra mass contributes towards a gain in stiffness. The additional vertical loading may also contribute to an increase in lateral stiffness. Later tests (I-L-21 to I-L-28) made use of the upper 1.7g accelerometer. An example Fourier transform with the EMV attached is shown in Figure 5.8, which agrees well with the lower accelerometer peak at 83 Hz. The pile was removed and reburied between tests I-L-14 and I-L-15 and tests I-L-20 and I-L-21.

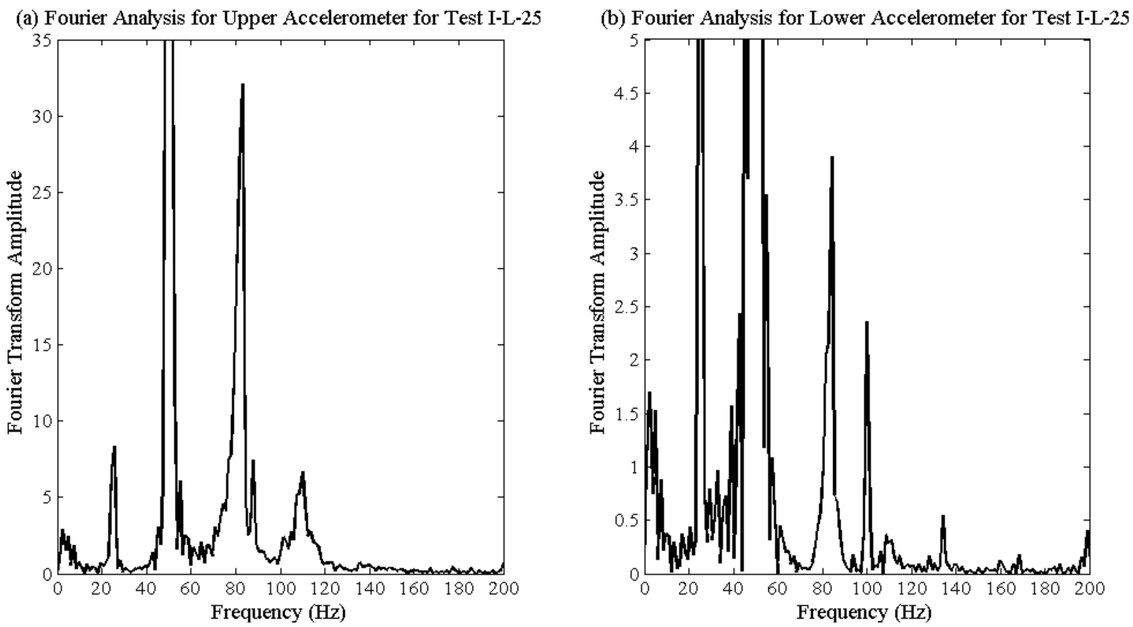

Figure 5.8. Fourier Analyses of Both 1.7g Accelerometers for an Impulse Test in Loose Sand

Tests I-L-29 to I-L-34 were carried out with the base plate, once the noise issue had been resolved, with two 1.7g accelerometers. This gives clearer time plots, shown in Figure 5.9. The damping is difficult to measure accurately, but is found to be higher than for the cantilever tests at 13.2% for the lower accelerometer. The Fourier transform shown in Figure 5.10 lacks the noise component at 50 Hz, and finds peaks at 90 Hz for both accelerometers.

As the mass of the base plate is 0.272 kg, this frequency is as expected. Table 4.2 gives a summary of the impulse tests in loose sand, analysed at a frequency resolution of 1.22 Hz.

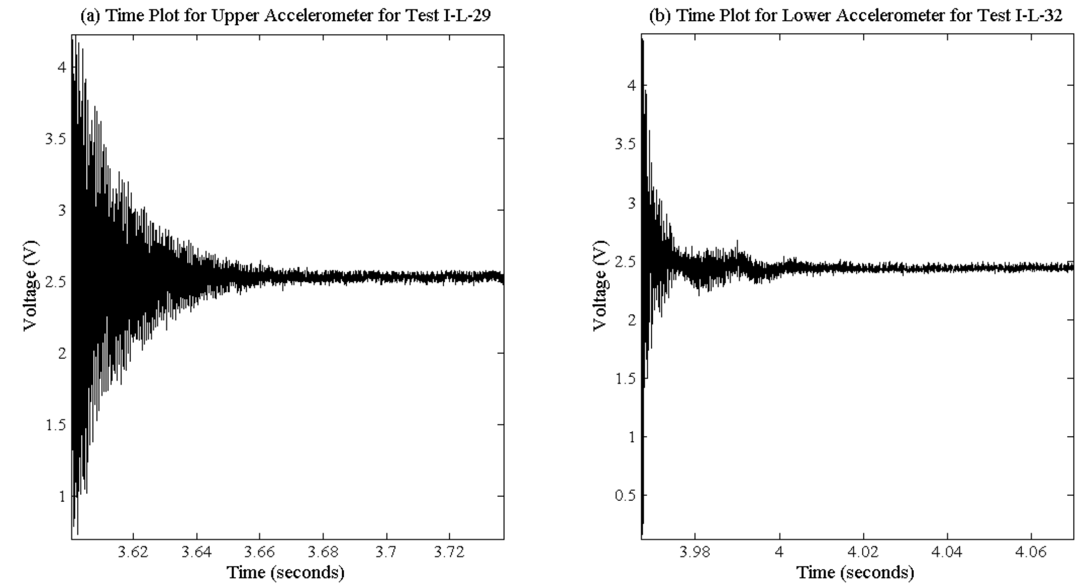

Figure 5.9. Example Time Plots with Noise Eliminated

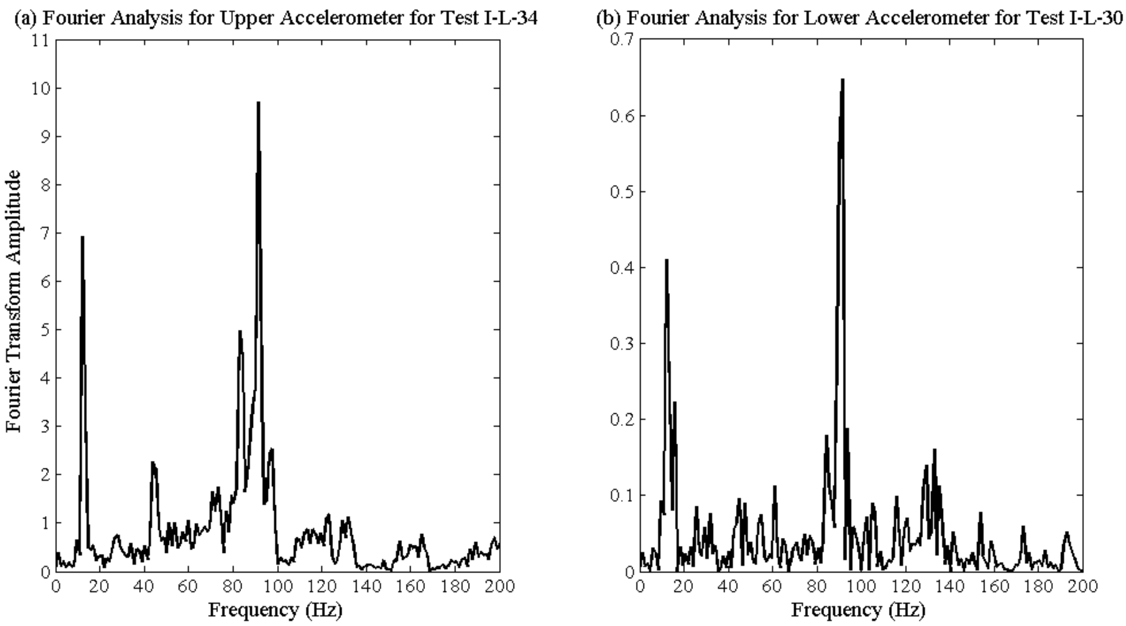

Figure 5.10. Example Fourier Analyses with Noise Eliminated

Generally there is good agreement between the results, small variations are due to the initial magnitude of the impulse applied. Each time the pile was removed and reburied, the embedment depth, and more critically the relative density of the sand was changed. This is represented by a double line in Table 5.2. This leads to small changes in the natural frequency of the monopile, which varies between 89 and 98 Hz without the added mass. This corresponds to a 21% change in stiffness, showing that this stiffness is sensitive to relative density and differences in cyclic loading.

Table 5.2. Summary of Loose Sand Impulse Test Results

Test Number	Upper Accelerometer Peak (Hz)	Lower Accelerometer Peak (Hz)	Added Mass (kg)
I-L-8	84	89	/
I-L-9	/	89	/
I-L-10	/	94	/
I-L-11	/	94	/
I-L-12	82	82	1.54
I-L-13	83	82	1.54
I-L-14	82	83	1.54
I-L-15	/	98	/
I-L-16	/	97	/
I-L-17	/	98	/
I-L-18	86	86	1.54
I-L-19	86	86	1.54
I-L-20	86	86	1.54
I-L-21	93	93	/
I-L-22	92	93	/
I-L-23	92	/	/
I-L-24	90	/	/
I-L-25	83	84	1.54
I-L-26	83	83	1.54
I-L-27	82	82	1.54
I-L-28	82	83	1.54
I-L-29	/	92	0.27
I-L-30	90	90	0.27
I-L-31	/	90	0.27
I-L-32	/	93	0.27
I-L-33	/	92	0.27
I-L-34	92	92	0.27

5.3 Dense Sand

Tests I-D-1 to I-D-9 were carried out with the base plate on top of the pile. Figure 5.11 shows example time traces for both accelerometers, with a damping ratio of 14.3% for the lower accelerometer. Figure 5.12 shows Fourier analyses for a range of tests. In order to find the correct frequency of the monopile, a large impulse was applied to the side of the tub. A dominant peak in Figure 5.13 at 127 Hz suggests that this is a natural frequency of the soil-tub system. In Test I-D-4, the impulse was applied to the top of the pile, whereas in Test I-D-8, the impulse was applied to the base plate itself, increasing the presence of the peak at 167 Hz in Figure 5.12a, suggesting that this is a frequency related to the base plate. It would appear that 156 Hz is the natural frequency of interest. Between tests I-D-3 and I-D-4 an increase of 3% in frequency and therefore 7% in stiffness is seen. In this period, three discarded tests were performed, in which a large impulse was applied to the pile using a spanner. It is thought that this significantly displaced the pile, increasing the soil stiffness.

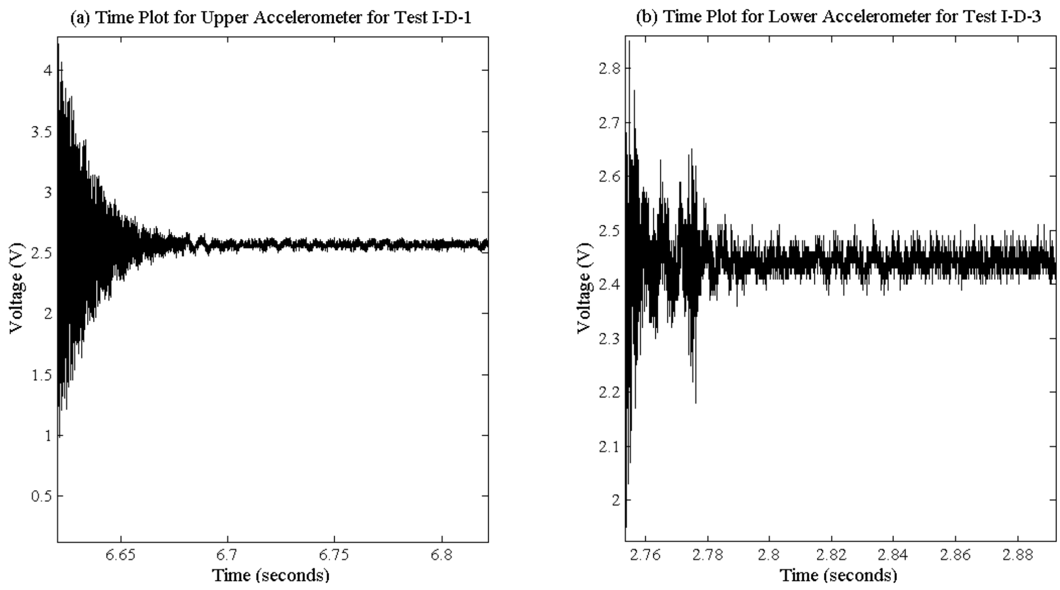

Figure 5.11. Example Time Plots for Tests in Dense Sand

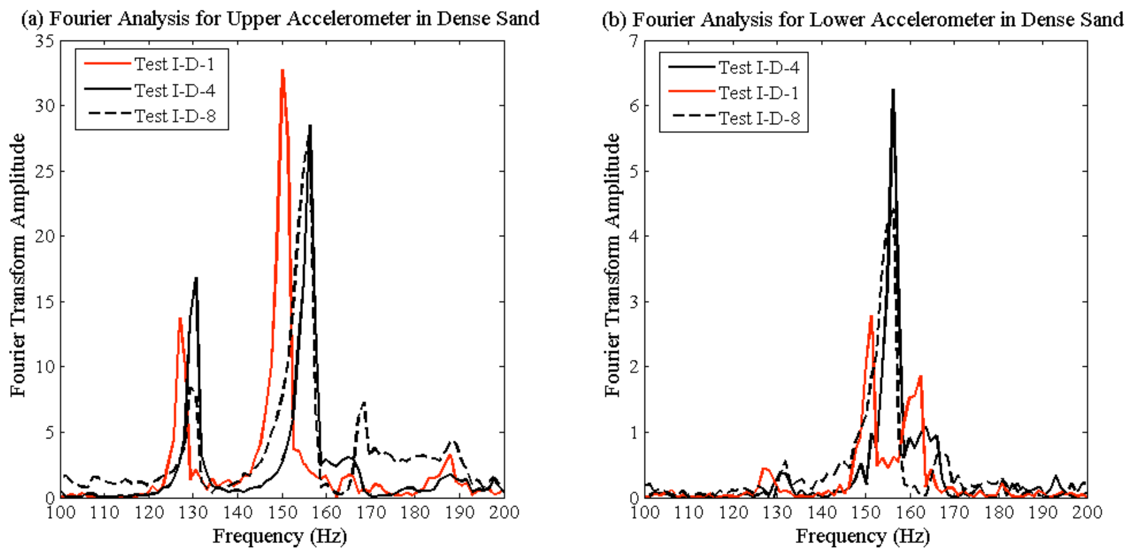

Figure 5.12. Fourier Analyses for a Range of Impulse Tests in Dense Sand

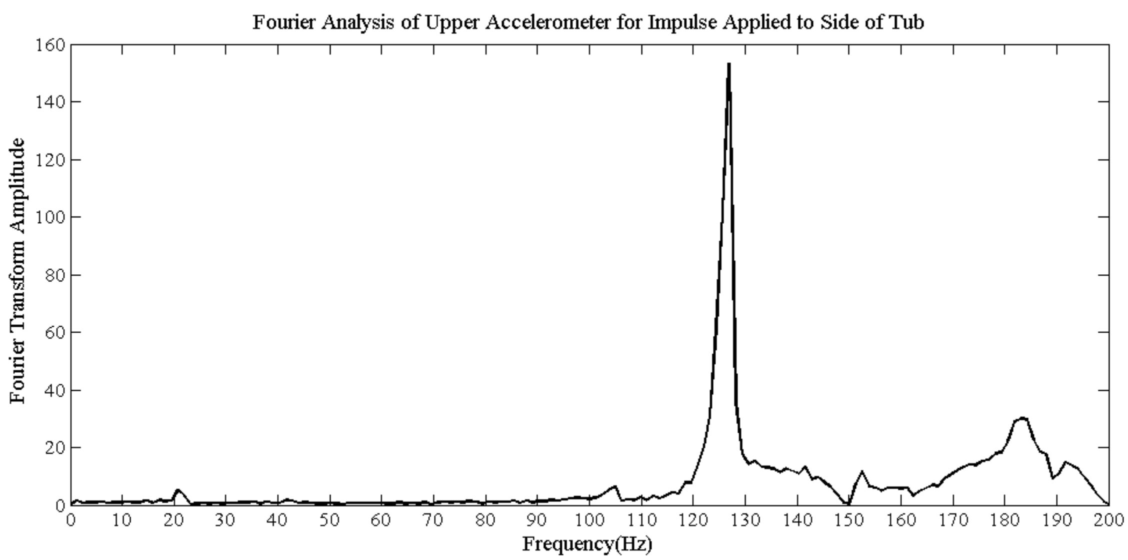

Figure 5.13. Fourier Analysis for Impulse Applied to Side of Tub

Table 5.3 gives a full summary of the results of dense sand impulse tests, with all Fourier analyses carried out with a frequency resolution of 1.22 Hz and an added mass of 0.272 kg.

Table 5.3. Summary of Dense Sand Impulse Test Results

Test Number	Upper Accelerometer Peak (Hz)	Lower Accelerometer Peak (Hz)
I-D-1	150	151
I-D-2	150	151
I-D-3	151	151
I-D-4	156	156
I-D-5	156	156
I-D-6	156	156
I-D-7	155	155
I-D-8	156	156
I-D-9	156	156

5.4 Reduced Embedment

The results of tests carried out on the monopile with an embedment of 185 mm in dense sand are shown and discussed in Section 6.2.3, in order to compare them with the equivalent tests carried out in clay.

5.5 Comparison with Model

For a direct comparison between the loose and dense sand tests, the impulse tests with the base plate attached should be looked at. For sand of relative density 29%, the frequency was found to be 91 Hz. For sand of relative density 60%, the frequency was found to be 156 Hz. Assuming that the contributing mass, and therefore the rotation point, is the same for both tests, the dense sand is found to be 2.9 times stiffer than the loose sand. The model developed predicted natural frequencies of 63 Hz for loose sand and 123 Hz for dense sand with no added mass, and therefore underestimates the stiffness for both. The added mass of the EMV reduces the loose sand predicted frequency to 28 Hz, but does not take into account the expected increase in stiffness with smaller displacements.

5.6 Evaluation of Impulse Tests

The pile-soil system is non-linear and dependent on the force applied, and the magnitude of an impulse cannot be directly compared to the amplitude of a harmonic force. As the response of the pile dies down, its frequency will increase as the amplitude of oscillation decreases. Therefore, a Fourier analysis of a longer sample finds a higher frequency, but gives better frequency resolution. Harmonic tests give a better idea of how the pile behaves under cyclic loading experience in the field. Methods discussed here to isolate the ‘correct’ natural frequency from impulse tests include comparison with reference cantilever tests, the addition of extra mass, and changing the application point of the impulse.

A piston device consisting of springs and a release mechanism shown in Figure 5.14 could be used to apply a more consistent impulse to the pile, this would improve comparison between tests. Alternatively, a step function of short duration could be applied using the piezo-electric actuator.

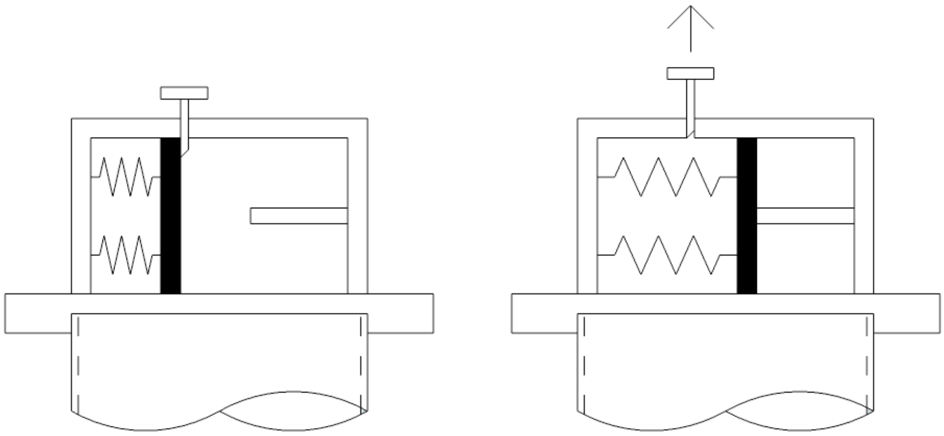

Figure 5.14 - Piston device for applying impulse to monopile

6 Harmonic Tests

6.1 Eccentric Mass Vibrator

The lower accelerometer was not sensitive enough to pick up a response for a force amplitude of 10.8 N applied by the EMV, so the amplitude was doubled. An example time plot for the upper accelerometer and both frequency plots for a ‘switch-off’ test are shown in Figure 6.1. The lower accelerometer time plot is not shown as it is dominated by noise at 50 Hz. The Fourier analysis shows a peak at 42 Hz for both accelerometers representing the average run-down frequency of the EMV, and a peak representing noise at 50 Hz for the lower accelerometer. It is difficult to say if the peak at 85 Hz corresponds to a harmonic of the 42 Hz peak or resonance of the pile. The EMV frequency dies down too quickly to find a peak in the range 0 to 50 Hz, and controlled frequency tests described in Section 6.2 are more useful. The EMV is nevertheless useful for applying cyclic loading in all directions between impulse tests to find changes in stiffness, even though this is not representative of the one-way cyclic loading experienced by offshore wind turbine monopiles.

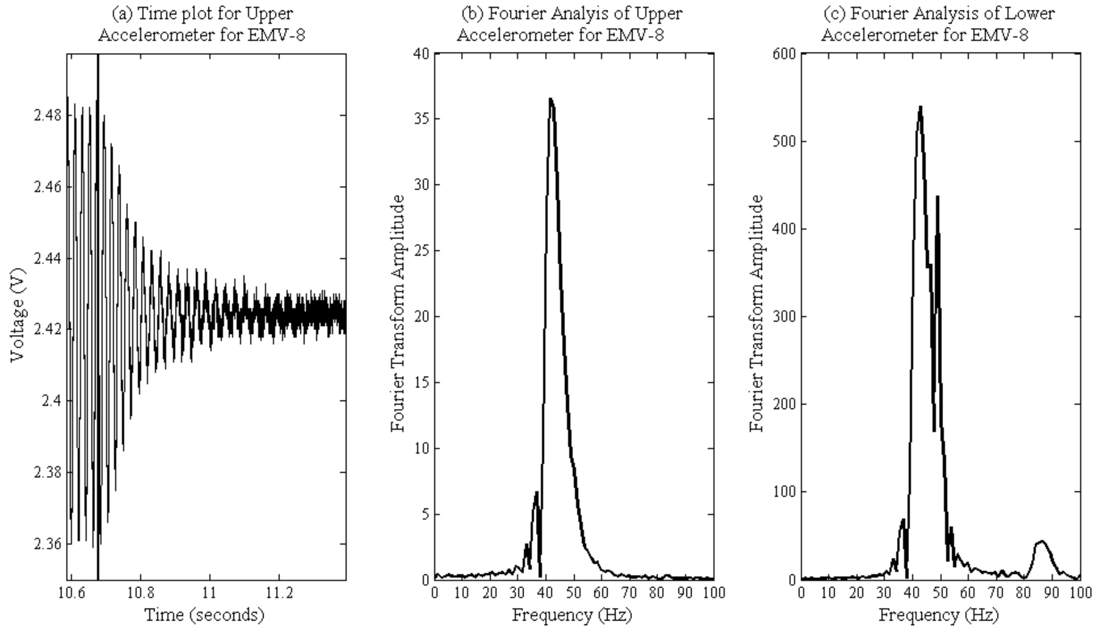

Figure 6.1. Results of EMV Tests

6.2 Piezo-electric Actuator

6.2.1 Cantilever Tests

Tests H-1 to H-39 were carried out on the pile as a cantilever, with 5-second samples taken at frequencies between 13 and 110 Hz at an input voltage of 6 V peak-to-peak. Figure 5.2 shows example time plots from the upper 1.7g accelerometer at 30 Hz (a) and 80 Hz (b).

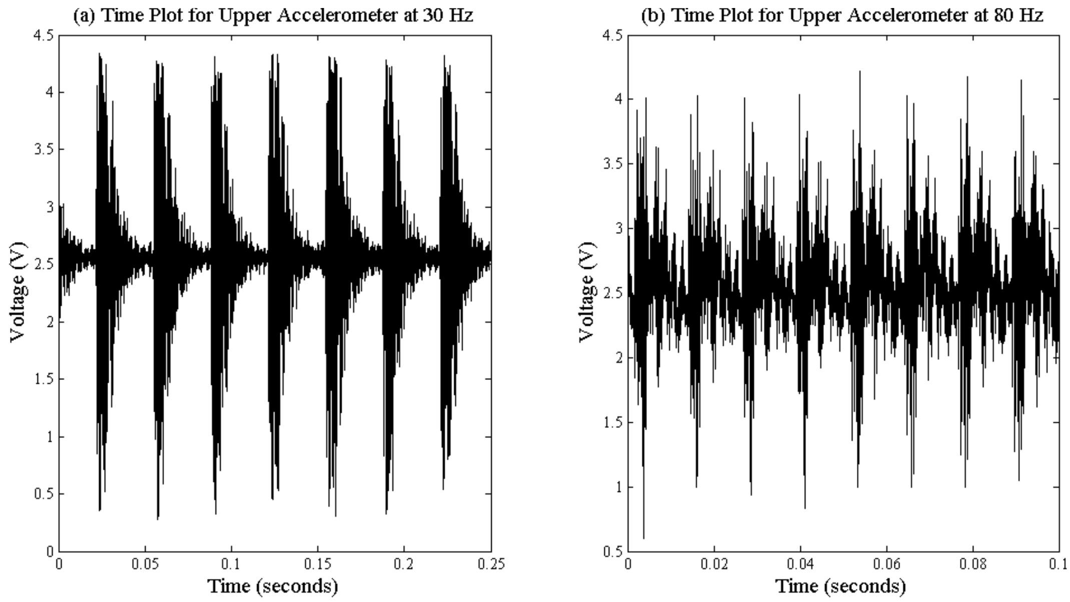

Figure 6.2. Response of the Monopile to Harmonic Loading

The response of the pile is equivalent to a series of impulses spaced at time intervals equivalent to the reciprocal of the forcing frequency. An alternative to this load control test is a displacement control test in which a sinusoidal response is forced. However, this is less representative of the loading experienced by the monopile. Two methods are used to analyse the samples. The first is to take the root mean square of the signal, this gives an idea of the amplitude of the signal at each forcing frequency. The second is to take a Fourier analysis of each sample and record the amplitude at the forcing frequency, and is the preferred method. The former method is used at lower forcing frequencies, as the Fourier analysis does not pick up these frequencies. Figure 6.3 shows the low frequency response for tests H-1 to H-15 for both accelerometers. There is a ‘cut-in’ frequency at around 15 Hz at which the pile begins to respond. After this there is a small peak before the response settles down. It is shown for later tests in sand and clay that this is a property of the actuator used.

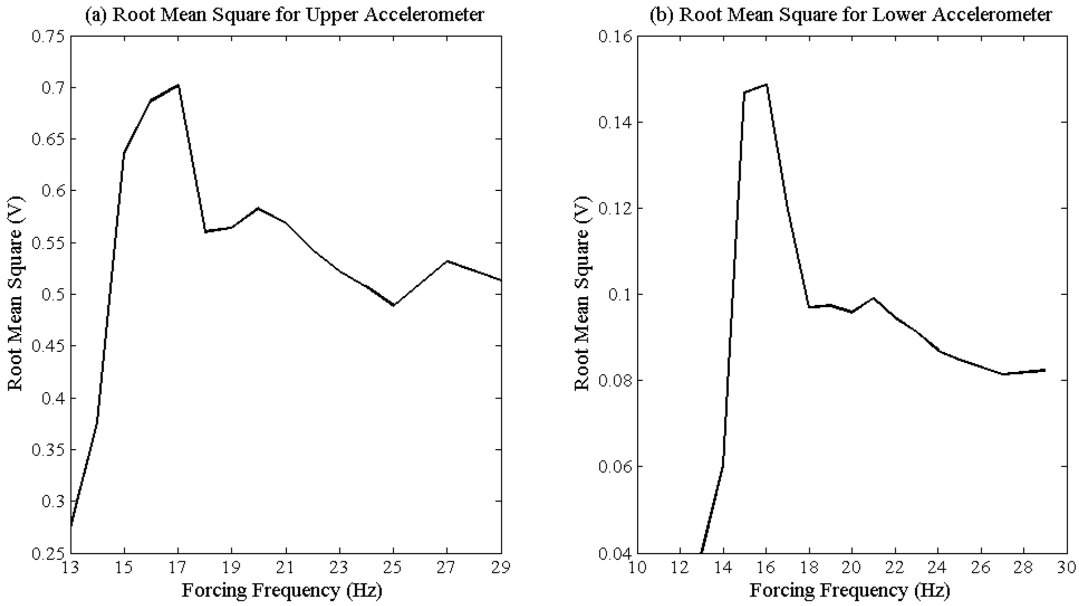

Figure 6.3. Root Mean Square of Response at Low Frequencies

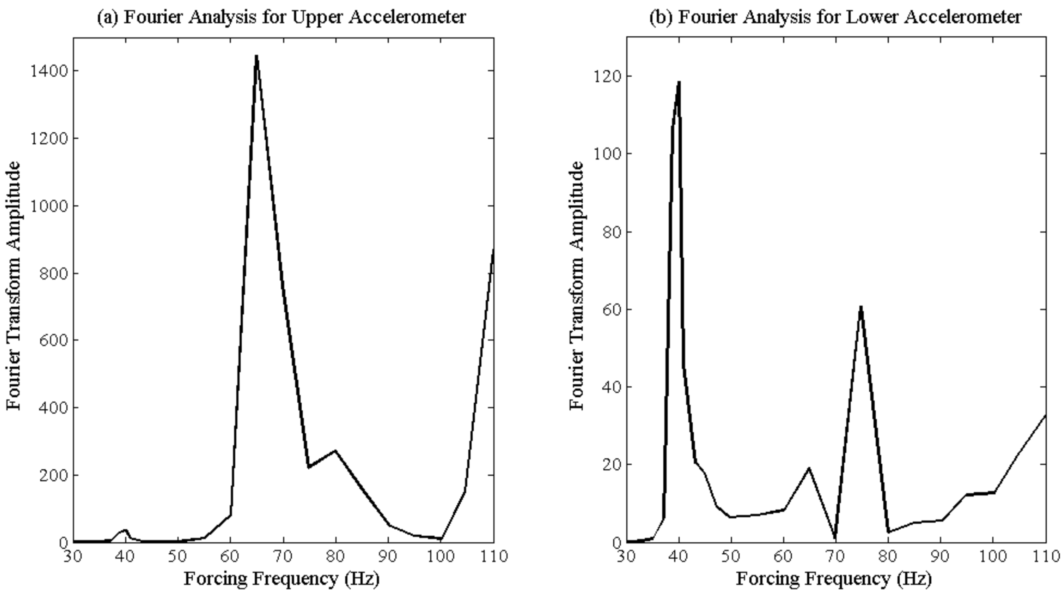

Figure 6.4. Fourier Analyses of Cantilever Harmonic Tests

Figure 6.4 shows the results of Fourier analyses for tests H-16 to H-39 for both accelerometers. The upper accelerometer shows a peak predominantly at 65 Hz. The lower accelerometer has peaks at 40 and 75 Hz. These results can be directly compared with the first impulse test in Figure 5.2, carried out with the same base fixity. Similar peaks were found at 40.3 and 70.8 Hz, and these were shown to change with the clamping conditions. The flexural natural frequency was found to be 130 Hz, and the frequency responses in Figures 5.3a and b can be seen to increase after 105 Hz, projecting up to this peak.

6.2.2 Loose Sand Tests

A similar time response was seen for tests in loose sand, consisting of a series of impulse responses. An increase in the amplitude of the signal was observed at between 75 and 95 Hz. The root mean square value of low frequency tests at 4.5 and 6 V peak-to-peak are plotted in Figure 6.5 for sand and clay tests. The peak is shown to increase from 15 to 16 Hz at 6 V to 22 to 23 Hz at 4.5 V. The 6 V peak agrees with that found for cantilever tests, and so is likely to be a property of the actuator, just after the ‘cut-in’ frequency.

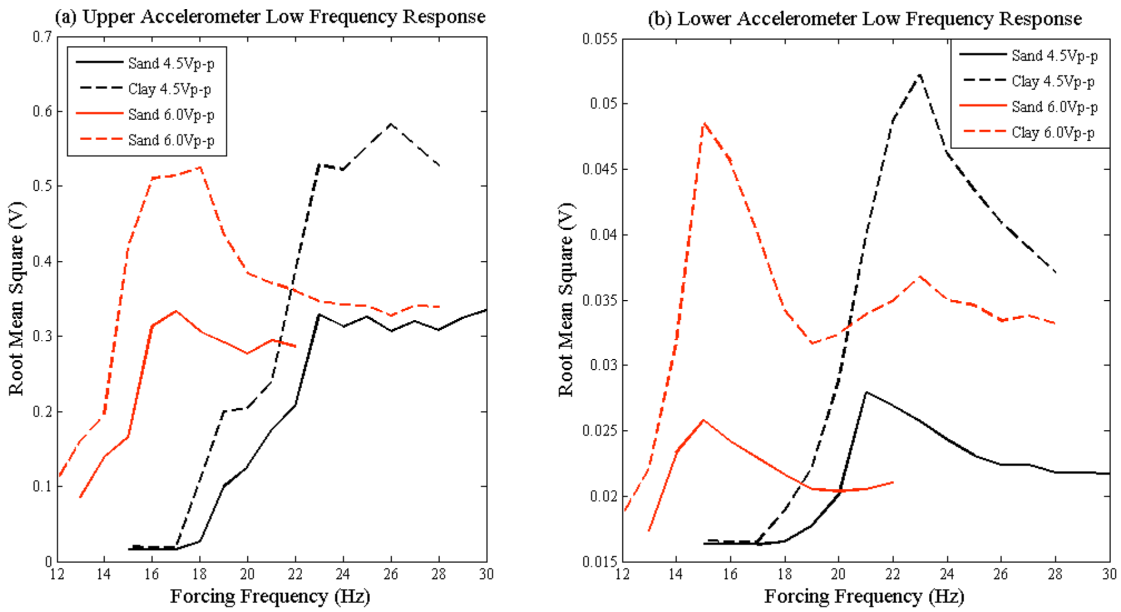

Figure 6.5. Root Mean Square of Low Frequency Response for Sand and Clay Tests

Focusing now on the natural frequency of the pile, the Fourier analyses for 6 V, 4.5 V and 3 V peak-to-peak tests are shown in Figures 6.6, 6.7 and 6.8 respectively. Later tests are plotted separately to check for frequency changes with cyclic loading. Initial tests at 6 V, with a frequency spacing of 5 Hz, find the natural frequency to be 80 to 85 Hz. Further tests at 1 Hz spacing have a peak at 82 Hz for the upper accelerometer. The lower accelerometer gives a natural frequency close to 85 Hz. No visible change in frequency is seen with time. For 4.5 V tests, again there appears to be little change in stiffness between tests. The upper accelerometer finds a natural frequency of 85 Hz, and the lower a frequency of 86 to 87 Hz. Finally, 3 V tests at 5 Hz spacing find the frequency to be slightly higher again for both accelerometers.

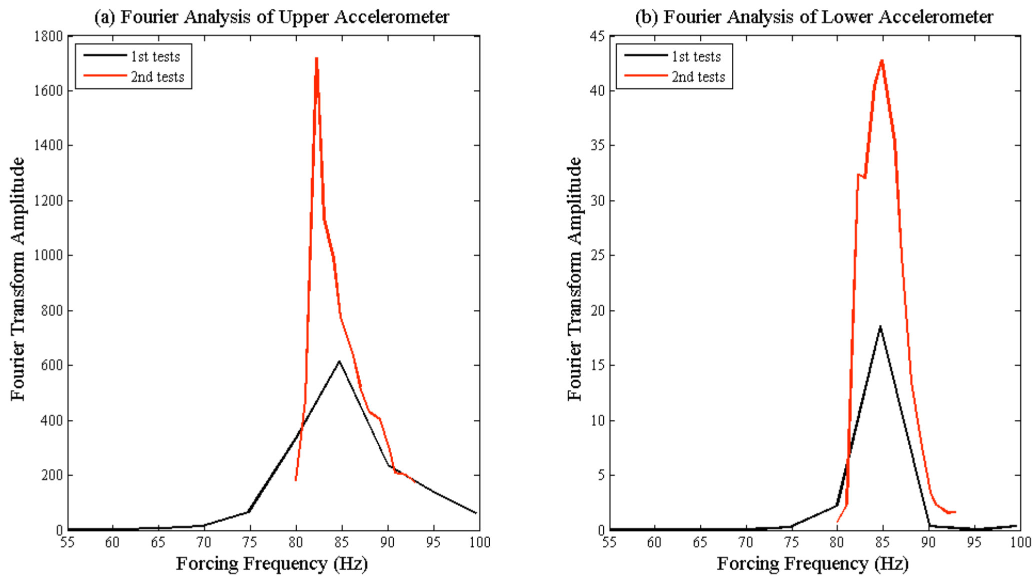

Figure 6.6. Fourier Analyses for 6 V p-p Harmonic Tests in Loose Sand

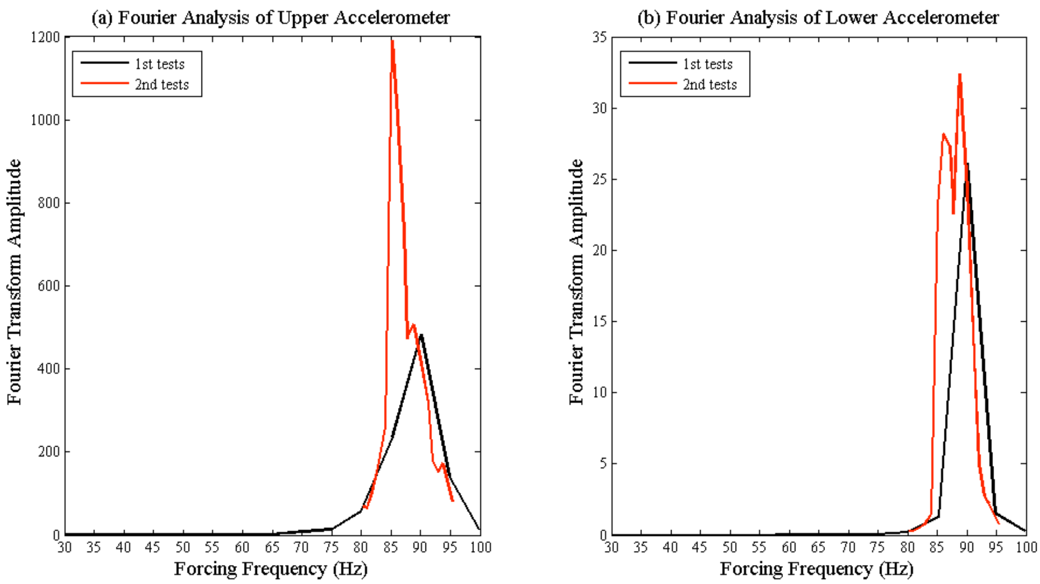

Figure 6.7. Fourier Analyses for 4.5 V p-p Harmonic Tests in Loose Sand

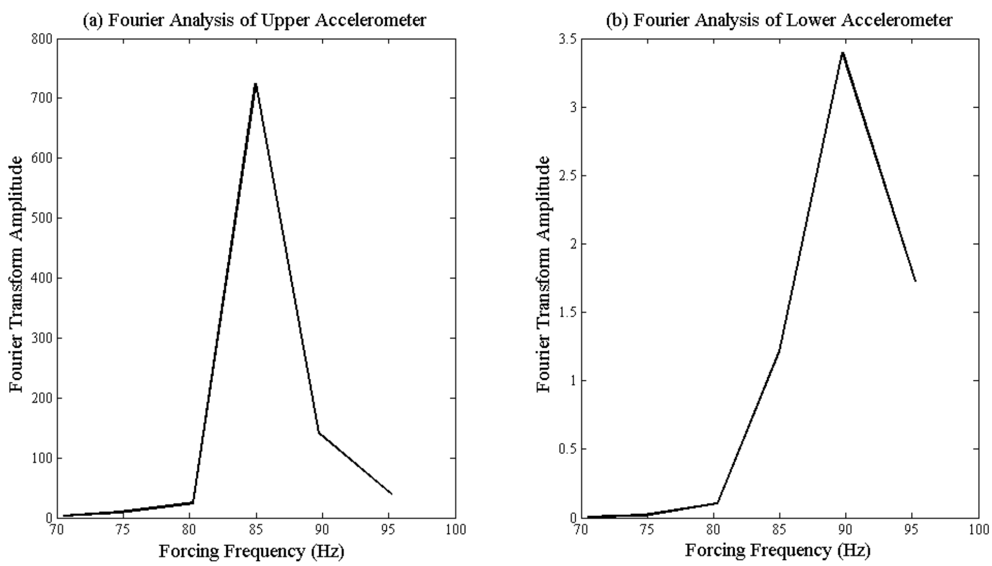

Figure 6.8. Fourier Analyses for 3 V p-p Harmonic Tests in Loose Sand

These tests were carried out in the same soil sample as impulse tests I-L-21 and I-L-28, which found a natural frequency of 93 Hz with no added mass and 83 Hz with 1.54 kg of added mass. For the actuator of mass 0.646 kg, the natural frequency is expected to fall between the two. This is confirmed by the lowest force (3 V) tests. The eccentricity of the loading is slightly greater than for impulse tests, which may lead to a slight decrease in stiffness. As the voltage, and hence force, is increased, the frequency drops. This is due to a decrease in secant stiffness with load. The rotation point may become deeper, increasing the stiffness to partly offset this. Preliminary cyclic tests using the actuator increased the stiffness of the sand fully, and the load level is not sufficient to see any further stiffness degradation or enhancement effects.

The acceleration of the actuator measured using an accelerometer is shown to be sinusoidal at 12 Hz and 80 Hz in Figure 6.9. Using the calibration factor 2.8 N/V suggested in Section 3.5, the force plots shown in Figure 6.10 are produced. The force is seen to increase quadratically with frequency, and this accelerometer also records the resonant peak. A force of just ±1.2 N is applied to the monopile near resonance at 6 V, smaller than the required ±7.4 N found from dimensional analysis. However, an increase in force still leads to a reduction in natural frequency, suggesting the stiffness is non-linear even at such small strains. The monopile was loaded in two-directions, and so no accumulated rotation of the pile was expected or found.

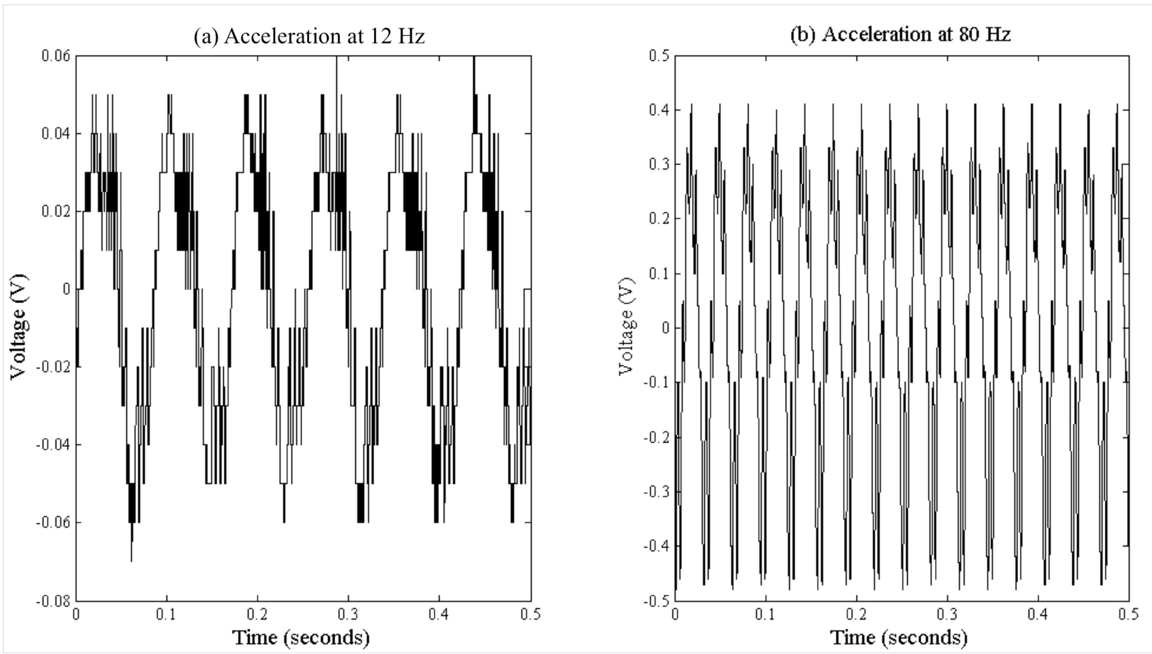

Figure 6.9. Acceleration of Actuator During Harmonic Tests

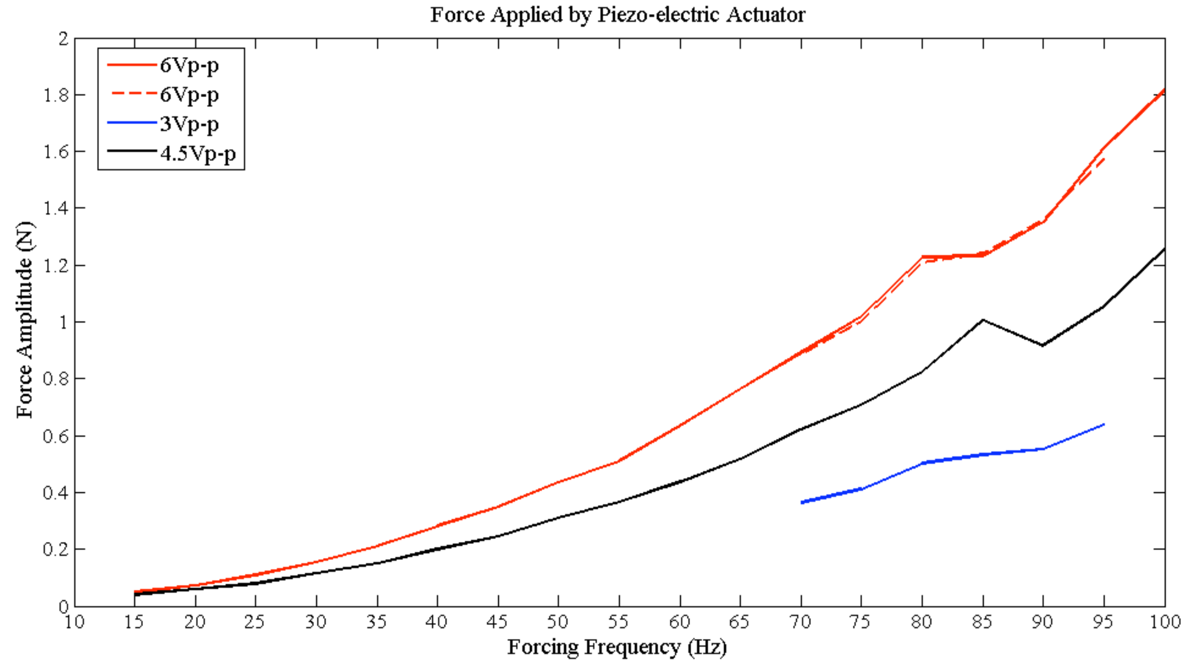

Figure 6.10. Amplitude of Harmonic Force Applied by Actuator

6.2.3 Clay Tests

Tests in clay were again found to have a similar time response and low frequency response to tests in sand. Fourier analysis plots for tests at 6 and 4.5 V peak-to-peak are shown in Figures 6.11 and 6.12 respectively. Tests were stopped abruptly after the peak was thought to be reached due to concerns over the amplitude of the oscillations. There is a lack of consistency, and variation of peaks with time. 6 V tests initially give a peak at 90 Hz, which then increases to 92 Hz. The peaks for 4.5 V tests vary greatly. The clay was not laterally confined in a tub, and dried out and cracked with time. The changes in stiffness are most likely due to these effects.

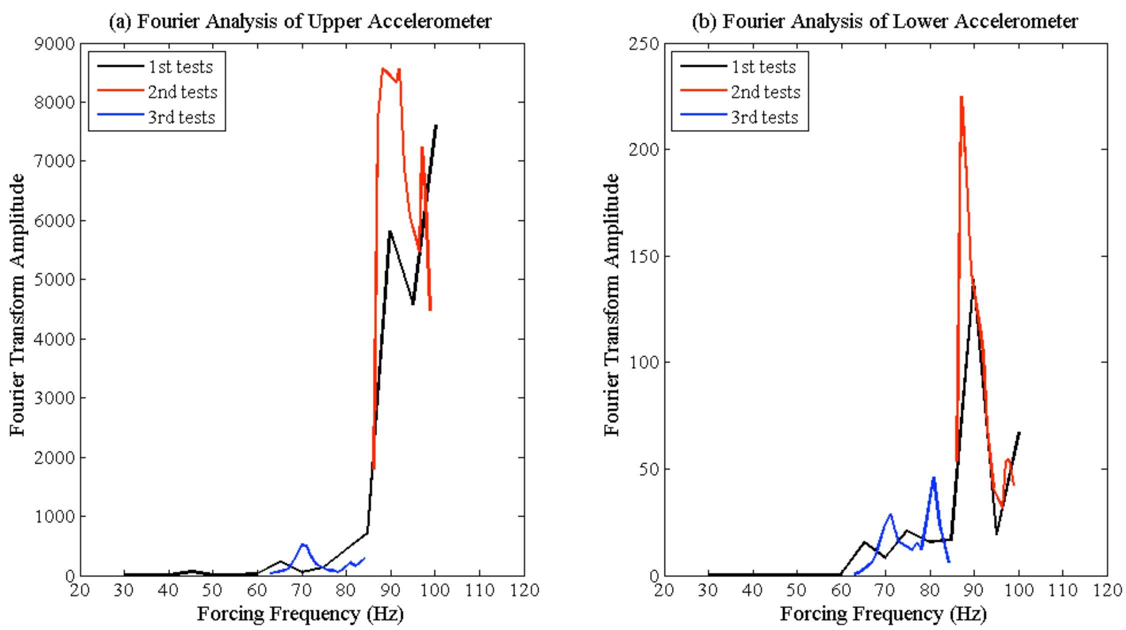

Figure 6.11. Fourier Analyses for 6 V p-p Harmonic Tests in Clay

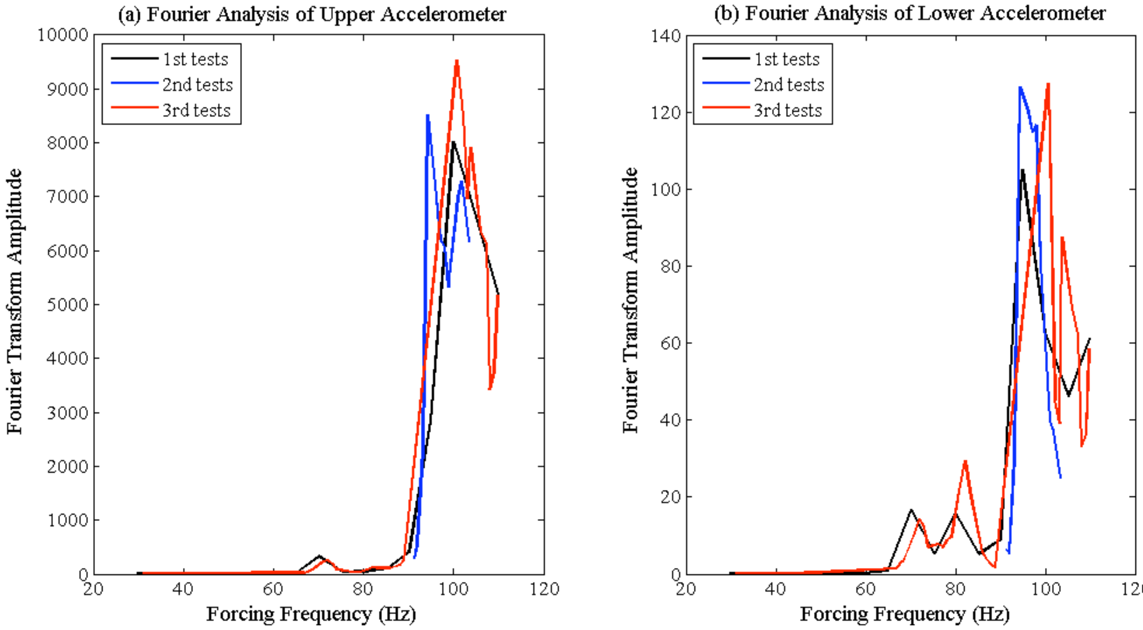

Figure 6.12. Fourier Analyses for 4.5 V p-p Harmonic Tests in Clay

Impulse tests carried out in dense sand for the same embedment with an added mass of 0.272 kg gave a natural frequency of around 103 Hz for all six tests (see Figure 6.13). With the reduced embedment (and therefore reduced stiffness), and increased mass of the pile above the surface, a much smaller natural frequency was expected than for larger embedment tests. The natural frequency was instead predicted to be a coupling of horizontal translation and rotational modes. The model predicted these to be 93 Hz and between 15 and 49 Hz respectively, which seems reasonable given the results. The effect of ignoring the flexural stiffness of the pile above the soil is expected to be more significant for these tests.

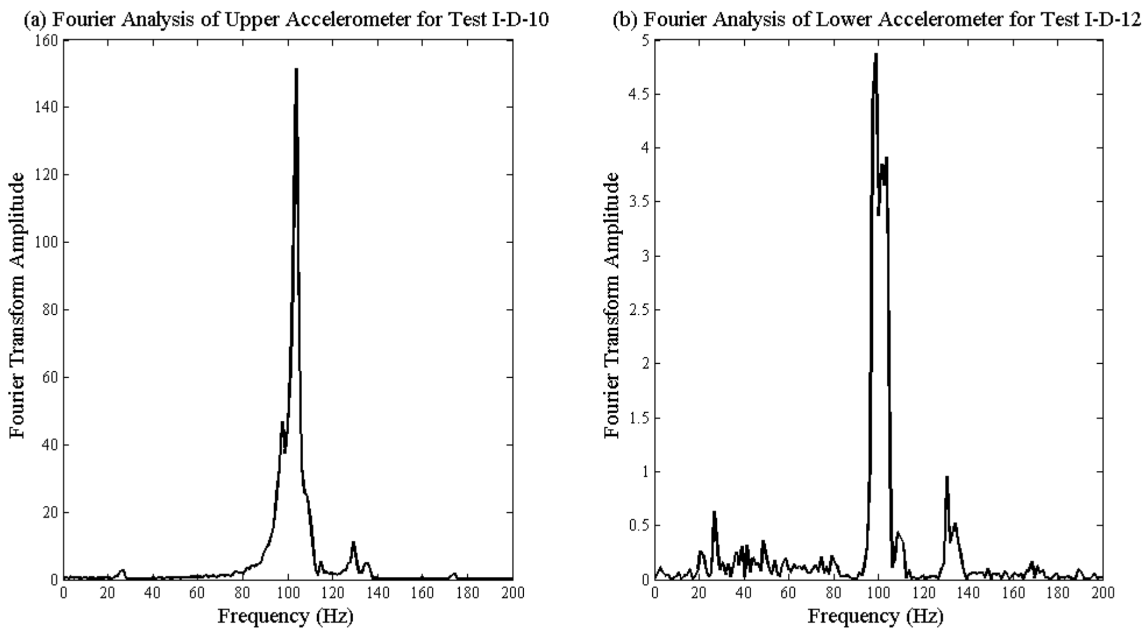

Figure 6.13. Example Fourier Analyses for Reduced Embedment Impulse Tests in Stiff Sand

It would appear that the clay has similar stiffness to the dense sand. Although sand is expected to be stiffer than clay, the clay was preconsolidated to 25 kPa, so with an effective unit weight of 10 kNm^{-3}, this corresponds to clay from a depth of 2.5 m. The dense sand has an average depth of just 0.2 m. However it is difficult to make comparisons between the clay and sand tests due to the differences in top mass. Also, the sand stiffness is expected to increase linearly with depth, whereas the undrained shear strength of the clay is assumed constant with depth, although the DNV (2010) guidelines suggest the lateral stiffness of the clay still increases with depth. Nevertheless, different lateral stiffness profiles are expected for clay and sand.

7 Limitations of Small-Scale Models

Although dimensionless groups were introduced to scale forces and eccentricities for small-scale models, many limitations still exist in using these models. For 1-g testing the main issue is that the confining pressure is very low as effective stresses are low. This leads to a much smaller shear modulus than in full-scale conditions. The p-y curves used were developed for piles of much greater depths than 0.4 m, and it is unclear how accurate these are at small depths. As the initial stiffness does not depend on the diameter of the pile in the code, applying them to such small diameter model monopiles may not be appropriate. One way to increase the confining pressure for small-scale models is to carry out centrifuge testing, which will be discussed in Section 8.3. However, the relative dimensions of the model to the soil particle sizes will never be the same as for full-scale testing; reducing the particle size to account for this will affect the behaviour significantly, especially for saturated tests. For full-scale monopiles it is expected that the relative density will increase with depth, and layers of different soil types may be found. Accepting these limitations, small-scale tests remain an easy and useful way of modelling large-scale frequency response problems, and can be used to supplement data from large scale field tests and centrifuge tests at the correct g-level.

8 Conclusions

It has been found that very few regulations exist for the design of rigid monopiles used to support offshore wind turbines. Guidelines tend to adopt p-y curves for lateral resistance used outside their confirmed range of slenderness. This is assumed to give safe predictions of the ultimate lateral resistance and conservative estimates of accumulated pile head rotation over the structure's lifetime. In order to predict the natural frequency of monopiles at low load levels relative to capacity, the initial stiffness of the p-y curves is important. A single degree of freedom model has been developed to predict the natural frequency for the rotation mode, assuming a rigid body mode shape and using p-y curves for the lateral resistance of the soil. This underestimates the natural frequency for small-scale tests in loose and dense sand states. The model is basic, and does not take into account base effects or the non-linear nature of the soil at small strains. The model is further used to predict the horizontal fundamental frequency, with a constant displacement assumed along the pile. For piles of low embedment and high eccentricity of loading, a coupling between the two modes was hypothesised, with experimental data showing some agreement.

8.1 Impulse Tests

In initial tests on the pile as a cantilever, finding fundamental frequencies of the pile proved difficult, as these were very sensitive to the degree of fixity and clamping force at the base of the cantilever. Methods were introduced to isolate the 'correct' natural frequency of the embedded pile. The most successful of these was adding extra mass, and finding peaks which decreased as a result. Another method was to vary the point of application of the impulse, and note the effect this had on any peaks. Good agreement was found between frequencies found from different accelerometers, and between tests. Cyclic loading was found to give an initial gain in stiffness of 11.6% after 6000 cycles for loose sand. No long-term changes in the stiffness or natural frequency were observed. The natural frequency of the monopile was found to vary with small variations in the soil density and embedment depth, with which the natural frequency increased as expected. The dense sand (I_D=0.60) was found to be 2.9 times stiffer than the loose sand (I_D=0.29), compared with 3.9 from theoretical p-y curves. A longer sample is required for the Fourier analysis to give better frequency resolution, however this was found to increase the noise in the signal and slightly increase the natural frequency found. As the signal dies down, the displacement decreases and therefore the stiffness of the soil increases, giving a higher frequency. Impulse tests are useful to give an idea of the natural frequency, however the pile-soil system is highly non-linear and the magnitude of the impulse cannot be directly compared with the magnitude of a dynamic force.

8.2 Harmonic Tests

Results of harmonic tests carried out using a piezo-electric actuator agreed well with results from impulse tests. At very small input forces, the frequency was similar to that in the impulse tests as expected, and as the force was increased, the frequency dropped corresponding to a decrease in soil stiffness. Even at very small load levels compared with design loads, this effect was seen, suggesting that a monopile has a range of natural frequencies. As the forces applied were small, long-term changes in the stiffness of the soil were not observed. Tests in clay proved inconclusive, results were inconsistent due to drying out of the clay and insufficient confinement. Reduced embedment tests in clay and dense sand found a possible coupling of horizontal and rotational modes due to the higher eccentricity of loading.

8.3 Suggestions for Further Work

The key parameter to vary for future tests is the diameter. It is known that the stiffness of the pile increases with embedment depth, but the theory suggested by DNV (2010) guidelines that the initial stiffness is independent of pile diameter needs to be tested to supplement the results reported by Alderlieste (2011), who found an increase in stiffness with pile diameter. Tests could be carried out at 1-g in loose and dense sands keeping the embedment depth constant and varying the diameter to investigate this effect. Initial impulse tests could be applied to find an upper bound on the natural frequency, followed by harmonic tests to investigate the force effect. Current tests at the University of Cambridge are investigating the response of monopiles in sands, clays and layered soils in a centrifuge at 100-g. In a typical test, the pile is driven into the soil and then the lateral resistance is recorded using a static load test. A piezo-electric actuator is used to apply an impulse before and after an extended period of cyclic loading, to find the change in natural frequency with cyclic loading. The results of these tests are used to develop and check finite element models of the problem. Further to these experiments, harmonic tests could be carried out in the centrifuge to find how the dynamic response and dynamic stiffness vary with force, and the results could be compared to static load test results.

9 References

Achmus, M., Kuo Y. S. & Abdel-Rahman, K. (2009). Behavior of monopile foundations under cyclic lateral load. *Computers and Geotechnics* **36**, 725-735

Adhikari, S. & Bhattacharya, S. (2012). Dynamic analysis of wind turbine towers on flexible foundations. *Shock and Vibration* **19**, 37-56

Alderlieste, E. A. (2011). Experimental modelling of lateral loads on large diameter monopile foundations in sand, M.Sc. thesis, Delft University of Technology, Netherlands

Bhattacharya, S., Wood, D. M. & Lombardi, D. (2010). Similitude relationships for physical modelling of monopile-supported offshore wind turbines. *International Journal of Physical Modelling in Geotechnics* **11**, No. 2 58-68

Brodbaek, K. T., Moller, M., Sorensen, S. P. H. & Augustesen, A. H. (2009). Review of p-y relationships in cohesionless soil. Aalborg University, Denmark

BWEA (2012). www.bwea.com/offshore/index.html. Retrieved 15/05/2012

Byrne, B. W. & Houlsby, G. T. (2003). Foundations for Offshore Wind Turbine. *Philosophical Transactions: Mathematical, Physical and Engineering Sciences* **361**, No. 1813, 2909-2930

DNV (2010). *Design of Offshore Wind Turbine Structures*, DNV-OS-J101. Det Norske Veritas

Dong Energy. www.dongenergy.com/Gunfleetsands. Retrieved 15/05/2012

Kuhn, M. (2001). Dynamics and design optimisation of offshore wind energy conversion systems. Delft University Wind Energy Research Institute, Report 2001.002

LeBlanc, C. (2004). Design of Offshore Wind Turbine Support Structures. Ph.D. thesis, Aalborg University, Denmark

LeBlanc, C., Houlsby, G. T. & Byrne, B. W. (2010). Response of stiff piles in sand to long-term cyclic lateral loading. *Géotechnique* **60**, No. 2, 79-90

Long, J. & Vanneste, G. (1994). Effects of cyclic lateral loads on piles in sand. *Journal of Geotechnical Engineering* **120**, No. 1, 225-244

Mitrani, H. (2006). Liquefaction remediation techniques for existing buildings. Ph. D. Thesis, University of Cambridge

National Grid (2010). Seven Year Statement. www.nationalgrid.com/uk/Electricity/SYS. Retrieved 15/05/2012

Pairaudeau, H. (2011). Construction and Performance of Shafts. M. Eng. Project, University of Cambridge

Prakash, S. & Kumar, S. (1996). Nonlinear lateral pile deflection prediction in sands. *Journal of Geotechnical Engineering* **122**, 130-138

Randolph, M. F. (1981). The response of flexible piles to lateral loading. *Géotechnique* **31**, No. 2, 247-259

Reese, L., Cox, W. R. & Koop, F. D. (1974). Analysis of laterally loaded piles in sand. *Proceedings of the 6th Offshore Technology Conference, Houston* **2**, paper no. 2079

Verdure, L., Garnier, J. & Levacher, D. (2003). Lateral cyclic loading of single piles in sand. *International Journal of Physical Modelling in Geotechnics* **3**, 17-28

A Risk Assessment Retrospective

The main risks associated with this experiment were identified as follows:

- Use of electrical equipment with water. Tests were carried out in dry sand for ease and to reduce this risk. For tests in saturated clay, all electrical equipment was kept above the clay surface.

No injuries resulted. The following changes are suggested to the original risk assessment:

- Dust hazard during pouring and excavation of sand. A dust extractor was used to reduce the level of dust in the laboratory, and a respirator helmet was used to mitigate the risk of respiratory issues resulting.
- Heavy lifting of tub. A pallet truck was used to move the tub around the laboratory. Where necessary, a forklift truck was used by a trained driver.
- General awareness of potential dangers such as trip hazards and heavy lifting equipment in use within the laboratory.
- General awareness of other uses of the laboratory.
- All experiments were carried out within the laboratory working hours in the presence of a laboratory technician.